

---

# CHAPTER 10

---

# PULSE COMPRESSION RADAR

---

**Edward C. Farnett**  
**George H. Stevens**

*RCA Electronic Systems Department*  
*GE Aerospace*

---

## 10.1 INTRODUCTION

---

Pulse compression involves the transmission of a long coded pulse and the processing of the received echo to obtain a relatively narrow pulse. The increased detection capability of a long-pulse radar system is achieved while retaining the range resolution capability of a narrow-pulse system. Several advantages are obtained. Transmission of long pulses permits a more efficient use of the average power capability of the radar. Generation of high peak power signals is avoided. The average power of the radar may be increased without increasing the pulse repetition frequency (PRF) and, hence, decreasing the radar's unambiguous range. An increased system resolving capability in doppler is also obtained as a result of the use of the long pulse. In addition, the radar is less vulnerable to interfering signals that differ from the coded transmitted signal.

A long pulse may be generated from a narrow pulse. A narrow pulse contains a large number of frequency components with a precise phase relationship between them. If the relative phases are changed by a phase-distorting filter, the frequency components combine to produce a stretched, or expanded, pulse. This expanded pulse is the pulse that is transmitted. The received echo is processed in the receiver by a compression filter. The compression filter readjusts the relative phases of the frequency components so that a narrow or compressed pulse is again produced. The pulse compression ratio is the ratio of the width of the expanded pulse to that of the compressed pulse. The pulse compression ratio is also equal to the product of the time duration and the spectral bandwidth (time-bandwidth product) of the transmitted signal.

A pulse compression radar is a practical implementation of a matched-filter system. The coded signal may be represented either as a frequency response  $H(\omega)$  or as an impulse time response  $h(t)$  of a coding filter. In Fig. 10.1a, the coded signal is obtained by exciting the coding filter  $H(\omega)$  with a unit impulse. The received signal is fed to the matched filter, whose frequency response is the complex conjugate  $H^*(\omega)$  of the coding filter. The output of the matched-filter section is the compressed pulse, which is given by the inverse Fourier transform of the product of the signal spectrum  $H(\omega)$  and the matched-filter response  $H^*(\omega)$ :

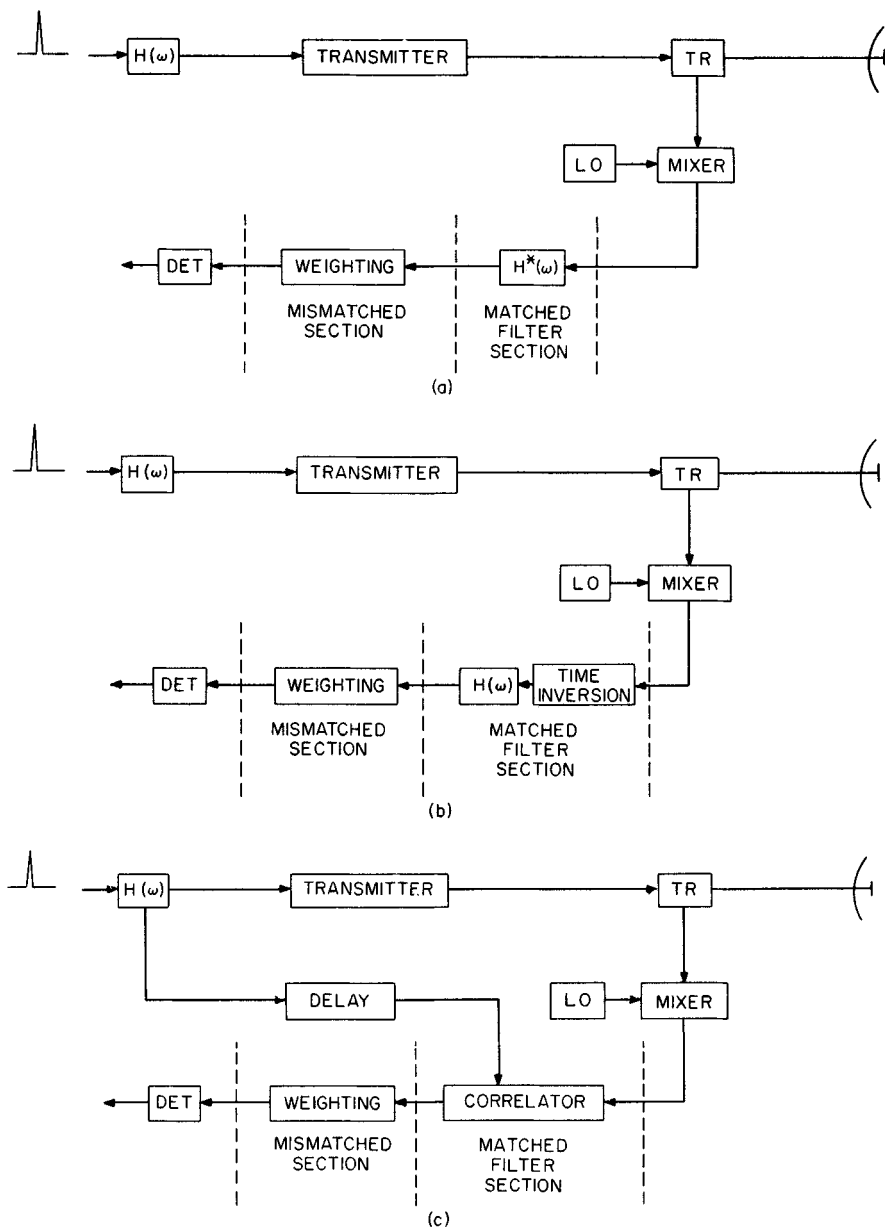


**FIG. 10.1** Pulse compression radar using (a) conjugate filters, (b) time inversion, and (c) correlation.

$$y(t) = \frac{1}{2\pi} \int_{-\infty}^{\infty} |H(\omega)|^2 e^{j\omega t} d\omega$$

The implementation of Fig. 10.1a uses filters which are conjugates of each other for the expansion and compression filters.

A filter is also matched to a signal if the signal is the complex conjugate of the time inverse of the filter's response to a unit impulse. This is achieved by applying the time inverse of the received signal to the compression filter, as shown in Fig. 10.1b. Identical filters may be used for both expansion and compression, or the same filter may be used for both expansion and compression with appropriate switching between the transmitting and receiving functions. The output of this matched filter is given by the convolution of the signal  $h(t)$  with the conjugate impulse response  $h^*(-t)$  of the matched filter:

$$y(t) = \int_{-\infty}^{\infty} h(\tau) h^*(t - \tau) d\tau$$

The matched filter results in a correlation of the received signal with the transmitted signal. Hence, correlation processing as shown in Fig. 10.1c is equivalent to matched filtering. In practice, multiple delays and correlators are used to cover the total range interval of interest.

The output of the matched filter consists of the compressed pulse accompanied by responses at other ranges, called time or range sidelobes. Frequency weighting of the output signals is usually employed to reduce these sidelobes. This results in a mismatched condition and leads to a degradation of the signal-to-noise output of the matched filter. In the presence of a doppler frequency shift, a bank of matched filters is required, with each filter matched to a different frequency so as to cover the band of expected doppler frequencies.

## 10.2 FACTORS AFFECTING CHOICE OF PULSE COMPRESSION SYSTEM

---

The choice of a pulse compression system is dependent upon the type of waveform selected and the method of generation and processing. The primary factors influencing the selection of a particular waveform are usually the radar requirements of range coverage, doppler coverage, range and doppler sidelobe levels, waveform flexibility, interference rejection, and signal-to-noise ratio (SNR). The methods of implementation are divided into two general classes, active and passive, depending upon whether active or passive techniques are used for generation and processing.

Active generation involves generating the waveform by phase or frequency modulation of a carrier without the occurrence of an actual time expansion. An example is digital phase control of a carrier. Passive generation involves exciting a device or network with a short pulse to produce a time-expanded coded waveform. An example is an expansion network composed of a surface-acoustic-wave (SAW) delay structure. Active processing involves mixing delayed replicas of the transmitted signal with the received signal and is a correlation-processing

approach. Passive processing involves the use of a compression network that is the conjugate of the expansion network and is a matched-filtering approach. Although a combination of active and passive techniques may be used in the same radar system, most systems employ the same type for generation and processing; e.g., a passive system uses both passive generation and passive processing.

The performance of common types of pulse compression systems is summarized in Table 10.1. The systems are compared on the assumption that information is extracted by processing a single waveform as opposed to multiple-pulse processing. The symbols  $B$  and  $T$  are used to denote, respectively, the bandwidth and the time duration of the transmitted waveform. Ripple loss refers to the  $SNR$  loss incurred in active systems because of the fluctuation or ripple in the  $SNR$  that occurs as a target moves from range cell to range cell. Clutter rejection performance of a single waveform is evaluated on the basis of doppler response rather than range resolution; pulse compression provides a means for realizing increased range resolution and, hence, greater clutter rejection. In applications where an insufficient doppler frequency shift occurs, range resolution is the chief means for seeing a target in clutter.

### 10.3 LINEAR FM

---

The linear-FM, or chirp, waveform is the easiest to generate. The compressed-pulse shape and  $SNR$  are fairly insensitive to doppler shifts. Because of its great popularity, more approaches for generating and processing linear FM have been developed than for any other coded waveform.<sup>1</sup> The major disadvantages are that (1) it has excessive range-doppler cross coupling which introduces errors unless either range or doppler is known or can be determined (i.e., a shift in doppler causes an apparent change in range and vice versa); and (2) weighting is usually required to reduce the time sidelobes of the compressed pulse to an acceptable level. Time and frequency weighting are nearly equivalent for linear FM and cause a 1 to 2 dB loss in  $SNR$ . Passive linear-FM generation and processing may be used as in Fig. 10.1a or b, where conjugate networks or a single network is employed. Active linear-FM generation and processing may be used as in Fig. 10.1c.

### 10.4 NONLINEAR FM

---

The nonlinear-FM waveform has attained little acceptance although it has several distinct advantages. The nonlinear-FM waveform requires no time or frequency weighting for range sidelobe suppression since the FM modulation of the waveform is designed to provide the desired amplitude spectrum. Matched-filter reception and low sidelobes become compatible in this design. Thus, the loss in signal-to-noise ratio associated with weighting by the usual mismatching techniques is eliminated. If a symmetrical FM modulation is used with time weighting to reduce the frequency sidelobes, the nonlinear-FM waveform will have a near-ideal ambiguity function. A symmetrical waveform typically has a frequency that increases (or decreases) with time during the first half of the pulse and decreases (or increases) during the last half of the pulse. A nonsymmetrical waveform is

**TABLE 10.1** Summary of Performance of Various Pulse Compression Implementations

	Linear FM		Nonlinear FM		Phase-coded	
	Active	Passive	Active	Passive	Active	Passive
Range coverage	Limited range coverage per active correlation processor.	Provides full range coverage.	Limited range coverage per active correlation processor.	Provides full range coverage.	Limited range coverage per active correlation processor.	Provides full range coverage.
Doppler coverage	Covers any doppler up to $\pm B/10$ , but a range error is introduced. <i>SNR</i> and time-sidelobe performance poor for larger doppler.		Multiple doppler channels required, spaced by $(1/T)$ Hz.			
Range sidelobe level	Requires weighting to reduce the range sidelobes below $(\sin x)/x$ falloff.		Good range sidelobes possible with no weighting. Sidelobes determined by waveform design.		Good range sidelobes. $N^{-1/2}$ for an $N$ -element code.	
Waveform flexibility	Bandwidth and pulse width can be varied.	Limited to one bandwidth and pulse width per compression network.	Bandwidth and pulse width can be varied.	Limited to one bandwidth and pulse width per compression network.	Bandwidth, pulse width, and code can be varied.	
Interference rejection	Poor clutter rejection.		Fair clutter rejection.		Fair clutter rejection.	
<i>SNR</i>	Reduced by weighting and by ripple loss versus range.	Reduced by weighting.	Reduced by ripple loss versus range.	No <i>SNR</i> loss.	Reduced by ripple loss versus range.	No <i>SNR</i> loss.
Comments	<ol style="list-style-type: none"> <li>Very popular with the advent of high-speed digital devices.</li> <li>Extremely wide bandwidths achievable.</li> </ol>	<ol style="list-style-type: none"> <li>Widely used in past.</li> <li>Well-developed technology.</li> </ol>	<ol style="list-style-type: none"> <li>Limited use.</li> <li>Waveform generation by digital means most popular.</li> </ol>	<ol style="list-style-type: none"> <li>Limited use.</li> <li>Extremely limited development.</li> </ol>	<ol style="list-style-type: none"> <li>Widely used.</li> <li>Waveform very easy to generate.</li> </ol>	<ol style="list-style-type: none"> <li>Limited use.</li> <li>Waveform moderately difficult to generate.</li> </ol>

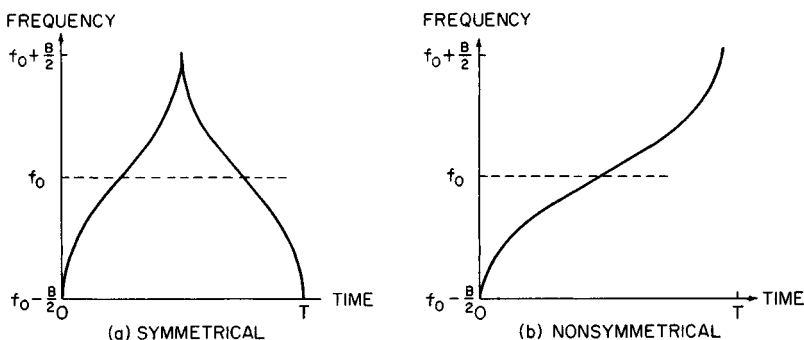


FIG. 10.2 Nonlinear-FM waveforms with 40 dB Taylor weighting.

obtained by using one-half of a symmetrical waveform (Fig. 10.2). However, the nonsymmetrical waveform retains some of the range-doppler cross coupling of the linear-FM waveform.

The disadvantages of the nonlinear-FM waveform are (1) greater system complexity, (2) limited development of nonlinear-FM generation devices, and (3) the necessity for a separate FM modulation design for each amplitude spectrum to achieve the required sidelobe level. Because of the sharpness of the ambiguity function, the nonlinear waveform is most useful in a tracking system where range and doppler are approximately known.

To achieve a 40 dB Taylor time-sidelobe pattern, the frequency-versus-time function of a nonsymmetrical transmitted pulse of bandwidth  $W$  is<sup>2</sup>

$$f(t) = W \left( \frac{t}{T} + \sum_{n=1}^7 K_n \left| \sin \left| \frac{2\pi n t}{T} \right| \right. \right)$$

where  $K_1 = -0.1145$   
 $K_2 = +0.0396$   
 $K_3 = -0.0202$   
 $K_4 = +0.0118$   
 $K_5 = -0.0082$   
 $K_6 = +0.0055$   
 $K_7 = -0.0040$

For a symmetrical frequency-versus-time function based on the above waveform, the first half ( $t \leq T/2$ ) of the frequency-versus-time function will be the  $f(t)$  given above, with  $T$  replaced with  $T/2$ . The last half ( $t \geq T/2$ ) of the frequency-versus-time function will be the  $f(t)$  above, with  $T$  replaced with  $T/2$  and  $t$  replaced with  $T/2 - t$ .

## 10.5 PULSE COMPRESSION DEVICES

Major advances are continually being made in the devices used in pulse compression radars. Significant advances are evident in the digital and SAW techniques.

These two techniques allow the implementation of more exotic signal waveforms such as nonlinear FM. The digital approach has blossomed because of the manifold increase in the computational speed and also because of the size reduction and the speed increase of the memory units. SAW technology has expanded because of the invention of the interdigital transducer,<sup>3</sup> which provides efficient transformation of an electrical signal into acoustic energy and vice versa. In spite of these advanced technologies, the most commonly used pulse compression waveforms are still the linear-FM and the phase-coded signals. Improved techniques have enhanced the processing of these "old standby" waveforms.

**Digital Pulse Compression.** Digital pulse compression techniques are routinely used for both the generation and the matched filtering of radar waveforms. The digital generator uses a predefined phase-versus-time profile to control the signal. This predefined profile may be stored in memory or be digitally generated by using appropriate constants. The matched filter may be implemented by using a digital correlator for any waveform or else a "stretch" approach for a linear-FM waveform.

Digital pulse compression has distinct features that determine its acceptability for a particular radar application. The major shortcoming of a digital approach is that its technology is restricted in bandwidths under 100 MHz. Frequency multiplication combined with stretch processing would increase this bandwidth limitation. Digital matched filtering usually requires multiple overlapped processing units for extended range coverage. The advantages of the digital approach are that long-duration waveforms present no problem, the results are extremely stable under a wide variety of operating conditions, and the same implementation could be used to handle multiple-waveform types.

Figure 10.3 shows the digital approach<sup>4</sup> for generating the radar waveform. This technique is normally used only for FM-type waveforms or polyphase-coded waveforms. Biphase coding can be achieved in a simpler manner, as shown in Sec. 10.6. The phase control element supplies digital samples of the in-phase component  $I$  and the quadrature component  $Q$ , which are converted to their analog equivalents. These phase samples may define the baseband components of the desired waveform, or they may define the waveform components on a low-frequency carrier. If the waveform is on a carrier, the balanced modulator is not required and the filtered components would be added directly. The sample-and-hold circuit is to remove the transients due to the nonzero transition time of the digital-to-analog ( $D/A$ ) converter. The low-pass filter smooths (or interpolates) the analog signal components between waveform samples to provide the equivalent of a much higher waveform-sampling rate. The  $I(t)$  component modulates a  $0^\circ$  carrier signal, and the  $Q(t)$  component modulates a  $90^\circ$  phase-shifted carrier signal. The desired waveform is the sum of the  $0^\circ$ -modulated carrier and the  $90^\circ$ -modulated carrier. As mentioned earlier, when the digital phase samples include the carrier component, the  $I$  and  $Q$  components are centered on this carrier fre-

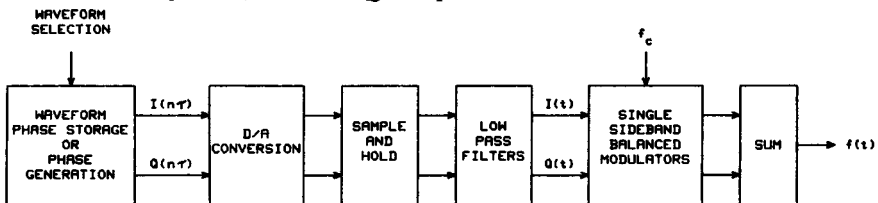


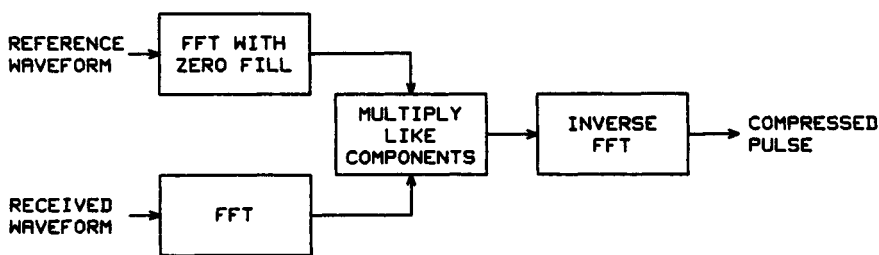
FIG. 10.3 Digital waveform generation.

quency and the low-pass filter can be replaced with a bandpass filter centered on the carrier.

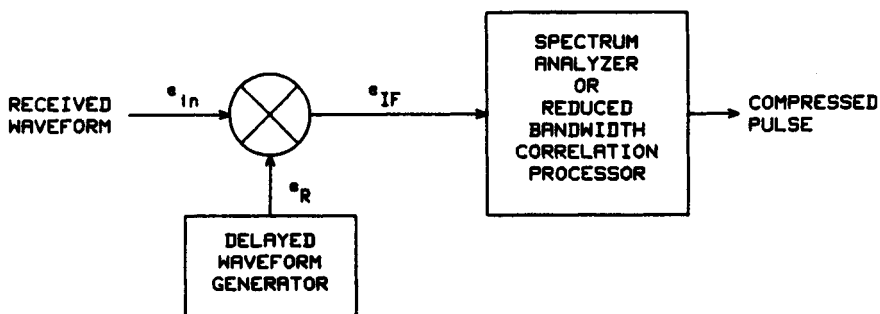
Digital waveform generators are very stable devices with a well-defined distortion. As a result, the generated waveform may be frequency-multiplied to achieve a much wider waveform bandwidth. With multiplication, the distortion components are increased in magnitude by the multiplication factor, and tighter control of the distortion is required.

When a linear-FM waveform is desired, the phase samples follow a quadratic pattern and can be generated by two cascaded digital integrators. The input digital command to the first integrator defines this quadratic phase function. The digital command to the second integrator is the output of the first integrator plus the desired carrier frequency. This carrier may be defined by the initial value of the first integrator. The desired initial phase of the waveform is the initial value of the second integrator or else may be added to the second-integrator output.

Figure 10.4 illustrates two digital approaches to providing the matched filter for a pulse compression waveform. These approaches provide only limited range coverage, and overlapped processors are needed for all-range performance. Figure 10.4a shows a digital implementation of a correlation processor that will provide matched-filter performance for any radar waveform. Figure 10.4b shows a



(a)



(b)

FIG. 10.4 Digital matched filter. (a) Correlation processor. (b) Stretch processor.



*stretch* processor for a linear-FM waveform. The delayed waveform has a bandwidth that is equal to or somewhat less than the transmitted waveform and a length that exceeds the duration of the transmitted waveform. This excess length equals the range window coverage.

The digital correlation processor<sup>5</sup> operates on the principle that the spectrum of the time convolution of two waveforms is equal to the product of the spectrum of these two signals. If  $M$  range samples are to be provided by one correlation processor, the number of samples in the fast Fourier transform (FFT) must equal  $M$  plus the number of samples in the reference waveform. These added  $M$  samples are filled with zeros in the reference waveform FFT. For extended range coverage, repeated correlation processor operations are required with range delays of  $M$  samples between adjacent operations. This correlation processor can be used with any waveform, and the reference waveform can be offset in doppler to achieve a matched filter at this doppler.

A stretch processor<sup>6</sup> can expand or contract the time scale of the compressed-pulse waveform within any defined time window. This general technique can be applied to any waveform, but it is much easier to use with a linear-FM waveform. For any waveform other than linear FM, an all-range pulse expansion approach is required in the received waveform path ahead of the mixer of Fig. 10.4b. Time contraction has not been applied to radar situations, as it requires an increased bandwidth for the compressed pulse. The stretch processing consideration will be restricted to time expansion of a linear-FM waveform.

Figure 10.4b shows the basic configuration of a time-expansion stretch processor for a linear-FM waveform. Let the received waveform be given by

$$e_{in} = A \operatorname{rect}\left(t - \frac{\tau_{in}}{T}\right) \sin [2\pi(f_0 + f_d)(t - \tau_{in}) + \pi\alpha_{in}(t - \tau_{in})^2 + \phi]$$

where  $\operatorname{rect}(X/T)$  is a unit amplitude pulse of duration  $T$  for  $|X| \leq T/2$ ;  $\tau_{in}$ ,  $T_{in}$ , and  $\alpha_{in}$  are the target time delay, the time pulse length, and the input frequency slope, respectively. The delayed waveform generator output will be

$$e_R = 2 \operatorname{rect}\left(t - \frac{\tau_r}{T_R}\right) \sin [2\pi f_R(t - \tau_R) + \pi\alpha_R(t - \tau_R)^2 + \phi]$$

where the constants are the reference waveform equivalent of the received waveform constants. The intermediate-frequency (IF) input to the pulse compressor can easily be shown to be

$$e_{IF} = A \operatorname{rect}\left(t - \frac{\tau_{in}}{T}\right) \operatorname{rect}\left(t - \frac{\tau_R}{T_R}\right) \cos [2\pi(f_0 + f_d - f_R)(t - \tau_{in}) + \pi(\alpha_{in} - \alpha_R)(t - \tau_{in})^2 + 2\pi\alpha_R(\tau_R - \tau_{in})(t - \tau_{in}) + \psi]$$

The resultant waveform is a reduced-frequency-slope linear-FM waveform with a target-range-dependent frequency offset riding on the doppler-shifted IF carrier frequency. Note that the frequency slope of the received waveform will be modified by the target's velocity.

For the special case where the two frequency slopes are equal, the IF

waveform is a constant-frequency pulse with an offset of  $f_d + \alpha_R (\tau_R - \tau_{in})$ . A spectrum analysis of this IF signal will yield the relative target range ( $\tau_R - \tau_{in}$ ) information. This frequency offset (exclusive of the target doppler) can be rewritten as  $B (\Delta T/T)$ , where  $B$  is the transmitted waveform bandwidth and  $\Delta T$  is the time separation between the two waveforms. If the waveform bandwidth is 1 GHz and the analyzer can process only a 10-MHz bandwidth, the range coverage is restricted to under 1 percent of the transmitted waveform length. To increase the range coverage, a wider processing bandwidth is required. This stretch approach allows the full range resolution of a wide-bandwidth waveform to be realized with a restricted bandwidth processor. Note that the duration of the reference waveform should exceed the duration of the received waveform by the range processed interval, or else an  $S/N$  loss will occur.

A stretch processor with unequal-frequency-slope waveforms requires pulse compression of the residual linear FM. A linear FM with a frequency slope of  $\alpha_{in} - \alpha_R$  occurs at the target's range. This linear FM will be offset in frequency by  $\alpha_R \Delta T$ . With the range-doppler coupling of the linear-FM waveform, the apparent range of this target will be

$$\tau_{app} = -\alpha_R \Delta T / (\alpha_{in} - \alpha_R)$$

This results in a time-expansion factor of  $\alpha_R / (\alpha_{in} - \alpha_R)$  for the compressed pulse. Again the range coverage capability of the system depends on the processing bandwidth that can be implemented.

**Surface-Wave Pulse Compression.** A SAW pulse compression unit consists of an input transducer and an output transducer mounted on a piezoelectric substrate. These transducers are usually implemented as interdigital devices which consist of a metal film deposited on the surface of the acoustic medium. This metal film is made of fingers (see Fig. 10.5) that dictate the frequency characteristic of the unit. The input transducer converts an electrical signal into a sound wave with over 95 percent of the energy traveling along the surface of the medium. The output transducer taps a portion of this surface sound wave and converts it back into an electric signal.

The SAW device<sup>7-9</sup> has unique features that dictate its usefulness for a given radar application. The major shortcomings of the SAW approach are that the waveform length is restricted to under 200  $\mu s$  by the physical size of available crystals and that each waveform requires another design. The advantages of the SAW device are its compact size, the wide bandwidths that can be attained, the ability to tailor the transducers to a particular waveform, the all-range coverage of the device, and the low cost of reproducing a given design.

SAW pulse compression devices depend on the interdigital transducer finger locations or else the surface-etched grating to determine its bandpass characteristic. Figure 10.5 shows three types of filter determination approaches. Figure 10.5a has a wideband input transducer and a frequency-selective (dispersive) output transducer. When an impulse is applied to the input, the output signal is initially a low frequency that increases (based on the output transducer finger spacings) at later portions of the pulse. This results in an up-chirp waveform which would be a matched filter for a down-chirp transmitted waveform. In Figure 10.5b, both the input transducer and the output transducer are dispersive. This would result in the same impulse response as that of Fig. 10.5a. For a given crystal length and material, the waveform duration for approaches in Fig. 10.5a and b would be the same and is limited to the time that it takes an acoustic wave to

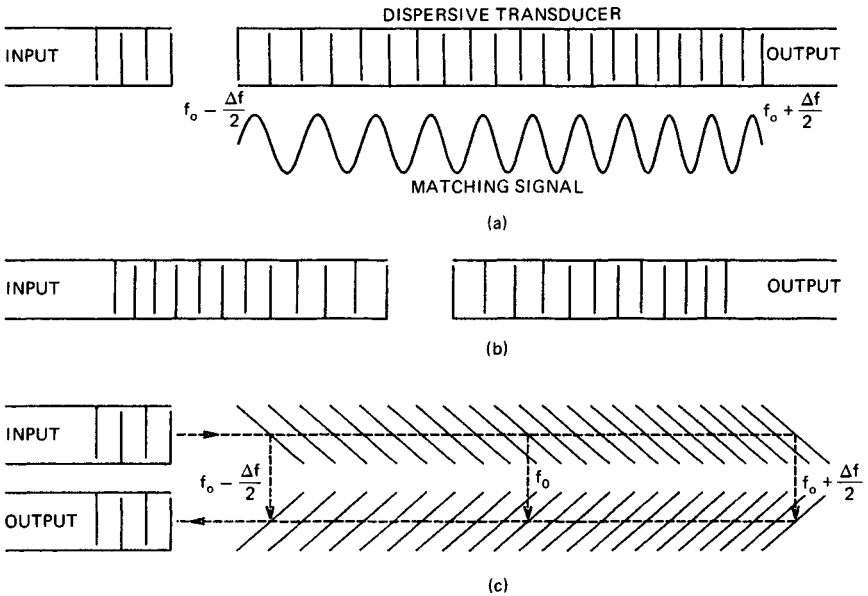


FIG. 10.5 SAW transducer types. (a) Dispersive output. (b) Both input and output dispersive. (c) Dispersive reflections.

traverse the crystal length. Figure 10.5c shows a reflection-array-compression (RAC) approach<sup>10</sup> which essentially doubles the achievable pulse length for the same crystal length. In an RAC, the input and output transducers have a broad bandwidth. A frequency-sensitive grating is etched on the crystal surface to reflect a portion of the surface-wave signal to the output transducer. This grating coupling does not have a significant impact on the surface-wave energy. Except for a 2:1 increase in the waveform duration, the impulse response of the RAC is the same as for approaches in Fig. 10.5a and b. Thus, these three approaches yield a similar impulse response.

Figure 10.6 shows a sketch of a SAW pulse compression device with dispersive input and output transducers. As the energy in a SAW device is concentrated in its surface wave, the SAW approach is much more efficient than bulk-wave devices, where the wave travels through the crystal. The propagation velocity of the surface wave is in the range of 1500 to 4000 m/s, depending on the crystal material, and allows a large delay in a compact device. Acoustic absorber material is required at the crystal edges to reduce the reflections and, hence, the spurious responses. Figure 10.7 shows the limit that can be expected from an SAW device and shows that bandwidths up to 1 GHz and delays up to 200  $\mu$ s are achievable. The upper frequency limit depends on the accuracy that can be achieved in the fabrication of the interdigital transducer. The SAW device must provide a response that is centered on a carrier, as the lowest frequency of operation is about 20 MHz and is limited by the crystal. A matched-filter SAW pulse compression device can use variable finger lengths to achieve frequency weighting, and this internal weighting can correct for the Fresnel wiggles<sup>11</sup> in the FM spectrum. With this correction, 43 dB time-sidelobe levels can be achieved

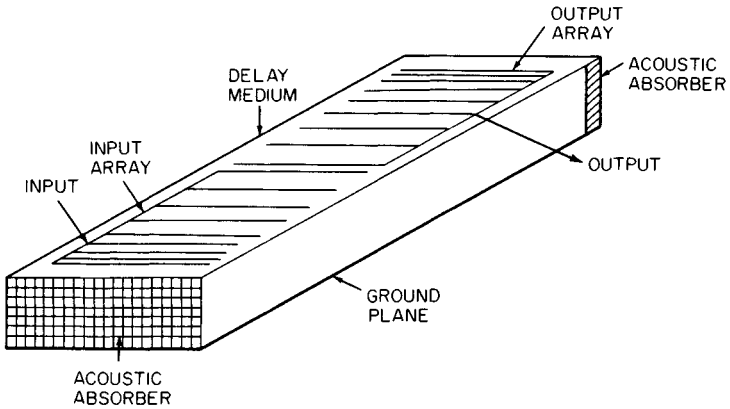


FIG. 10.6 Surface-wave delay line.

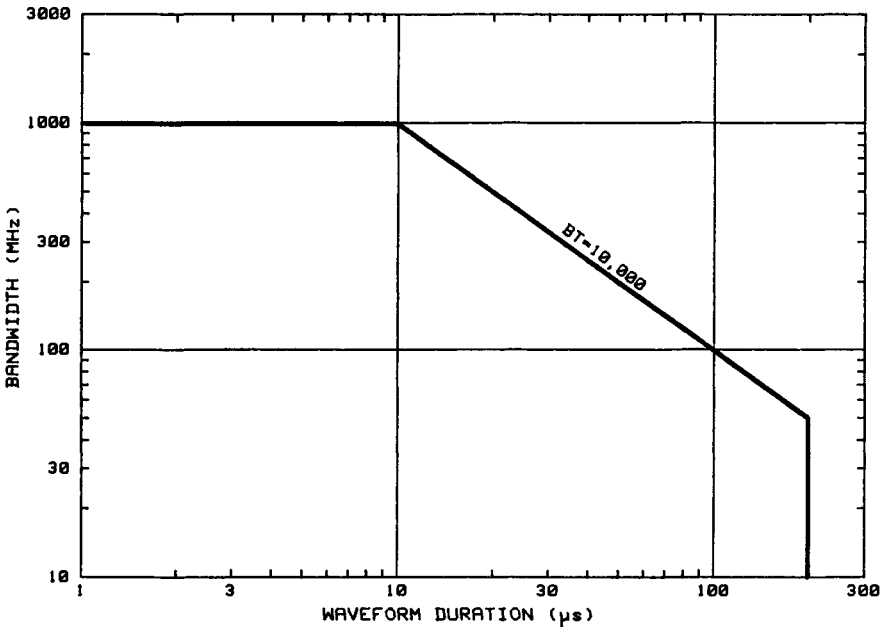


FIG. 10.7 Waveform limits for a SAW device.

for a linear-FM waveform with a  $BT$  as low as 15. The dynamic range is limited to under 80 dB by nonlinearities in the crystal material. The most common SAW materials are quartz and lithium niobate.

**Other Passive Linear-FM Devices.** Table 10.2 summarizes the general characteristics of several other passive devices that are used for linear-FM

**TABLE 10.2** Characteristics of Passive Linear-FM Devices

	$B$ , MHz	$T$ , $\mu$ s	$BT$	$f_0$ , MHz	Typical loss, dB	Typical spurious, dB
Aluminum strip delay line	1	500	200	5	15	-60
Steel strip delay line	20	350	500	45	70	-55
All-pass network	40	1000	300	25	25	-40
Perpendicular diffraction delay line	40	75	1000	100	30	-45
Surface-wave delay line	40	50	1000	100	70	-50
Wedge-type delay line	250	65	1000	500	50	-50
Folded-tape meander line	1000	1.5	1000	2000	25	-40
Waveguide operated near cutoff	1000	3	1000	5000	60	-25
YIG crystal	1000	10	2000	2000	70	-20

pulse compression. These passive devices fall into two broad classes: (1) bulk ultrasonic devices in which an electrical signal is converted into a sonic wave and propagates through the medium and (2) electrical devices that use the dispersive characteristic of an electrical network. The main objectives in designing and selecting a device are (1) a flat-amplitude characteristic over the bandwidth  $B$ , (2) a linear delay slope with a differential delay  $T$  across the bandwidth  $B$ , (3) minimum spurious responses and minimum distortion to achieve low sidelobes, and (4) a low insertion loss.

In a bulk ultrasonic device the input electrical signal is transformed into an acoustic wave, propagates through a medium at sonic speeds, and is then converted back to an electrical signal at the output. Since the wave propagates at sonic speeds, longer delays are achieved than with an electrical device of comparable size. A major disadvantage of ultrasonic devices is that the transducers required for coupling electrically to the acoustic medium are inefficient energy converters and hence cause high insertion losses. The most common types of bulk ultrasonic dispersive devices are (1) strip delay lines, (2) perpendicular diffraction delay lines, (3) wedge delay lines, and (4) yttrium iron garnet (YIG) crystals. The strip delay line and the YIG crystal depend on the dispersive nature of the medium for their operation. The other two types use a nondispersive medium and depend upon the diffraction characteristics of the input and output transducers for their operation; hence they are called grating-type delay lines.

A strip delay line<sup>12-15</sup> is made of a long, thin strip of material with transducers at opposite ends. Since the strips must be extremely thin (of the order of a few milli-inches), metal is selected because of its ruggedness. Aluminum and steel are the only metals that have found wide application. The dispersive strip delay line uses the phenomenon that if acoustic energy is propagated through a medium as a longitudinal wave, the medium exhibits a nearly linear delay-versus-frequency characteristic over an appreciable frequency range. The strip width is not critical as long as it is greater than 10 acoustic wavelengths. The thickness, however, is very critical and must be about one-half of an acoustic wavelength at a frequency equal to the center of the linear delay-versus-frequency characteristic. The length of the strip is a linear function of the differential delay required, but the bandwidth is independent of length. The differential delay corresponds to the time

separation between the initial frequency and the final frequency of the waveform and is usually equal to the expanded pulse width  $T$ .

Because the thickness is very critical and cannot be controlled adequately, the stripline is placed in an oven whose temperature is adjusted to control the final operating frequency. One side of the strip is treated with an absorbing material to prevent reflections which could excite a wave that is not longitudinal and could thus introduce spurious signals.

Aluminum strip delay lines have the lowest losses, but their center frequency and bandwidth must be kept low. It is necessary to operate these lines below about 5 MHz if differential delays of over 50  $\mu\text{s}$  are required. Aluminum lines have a midband delay of 7 to 10  $\mu\text{s}/\text{in}$ .

Steel strip delay lines have high losses but operate at higher center frequencies, permitting wider bandwidths. Steel lines have typical losses of 70 to 80 dB and operating frequencies between 5 and 45 MHz. Steel lines have midband delays of 9 to 12  $\mu\text{s}/\text{in}$ .

The perpendicular diffraction delay line<sup>13,14,16</sup> uses a nondispersive delay medium, such as quartz, with nonuniform input and output array transducers arranged on adjacent, perpendicular faces of the medium to produce the dispersion. The array element spacings decrease with increasing distance from the vertex of the right angle between the arrays. Thus only a positive slope of delay versus frequency can be produced. The bandwidth of the device is dictated by the array designs, and the delay is controlled by the size of the device. Errors in the array spacings produce phase errors which generate amplitude ripples and delay nonlinearities. Since many paths exist at a given frequency, these delay and amplitude errors tend to average out. Because of the averaging of the phase errors, the best delay linearity is achieved when the maximum number of grating lines is used. The center-frequency delay is limited to less than 75  $\mu\text{s}$  for normal lines and 225  $\mu\text{s}$  for polygonal lines because of limitations on the size of the quartz. In polygonal lines, the acoustic wave reflects off several reflecting faces in traveling from the input to the output array.

The wedge-type dispersive delay line<sup>14</sup> uses a wedge of quartz crystal and a frequency-selective receiver array to produce a linear delay-versus-frequency characteristic. The input transducer has a wide bandwidth, and the receiving-array elements are spaced in a quadratic manner. Reversal of the spacing of the output-array elements will change the output from an up-chirp waveform to a down-chirp waveform. The delay slope is dependent on the output-array configuration and the wedge angle. This device is fairly sensitive to grating phase errors since there is only one delay path per frequency.

YIG crystals<sup>15,17</sup> provide a dispersive microwave delay. YIG devices do not have a linear delay-versus-frequency characteristic, but their delay characteristic is very repeatable. The crystals require an external magnetic field, and the bandwidth and center frequency increase with the field strength. The delay of a YIG is determined by the crystal length. The maximum crystal length is limited to about 1.5 cm, corresponding to a delay of about 10  $\mu\text{s}$ .

In the electrical-network class of linear-FM waveform generators, a signal is passed through an electrical delay network designed to have a linear delay-versus-frequency characteristic. The most common electrical networks that are used to generate linear-FM waveforms are (1) all-pass networks, (2) folded-tape meander lines, and (3) waveguide operated near its cutoff frequency. The all-pass network is a low-frequency device that uses lumped constant elements. The other two networks operate at very high frequencies and depend upon distributed parameters for delay.

An all-pass time-delay network<sup>18,19</sup> is ideally a four-terminal lattice network with constant gain at all frequencies and a phase shift that varies with the square of the frequency to yield a constant delay slope. The networks have equal input and output impedances so that several networks can be cascaded to increase the differential delay.

The folded-tape meander line<sup>20</sup> is the UHF or microwave analog of the low-frequency, all-pass network. A meander line consists of a thin conducting tape extending back and forth midway between two ground planes. The space between tape meanders and between the tape and the ground plane is filled with dielectric material. The center frequency of a meander loop is the frequency at which the tape length is  $\lambda/4$ . The time delay per meander loop is a function of the dimensions of the loop and the distance from the ground plane. To achieve a linear delay-versus-frequency curve, several loops with staggered delay characteristics are used in series. The number of meander loops required is greater than  $B\Delta T$ .

Other microwave dispersive networks include a waveguide operated near its cutoff frequency and stripline all-pass networks. If a section of rectangular waveguide is operated above its cutoff frequency, the time delay through the waveguide decreases with frequency. Over a limited frequency band, delay is a linear function of frequency. The usable frequency band and the delay linearity are significantly improved by employing a tapered-waveguide structure. Since stripline all-pass networks are microwave counterparts of the low-frequency all-pass networks, the synthesis of these networks is usually based on the low-frequency approach.

**Voltage-Controlled Oscillator.** A voltage-controlled oscillator (VCO) is a frequency generation device in which the frequency varies with an applied voltage. Ideally, the frequency is a linear function of the applied voltage, but most devices have a linearity error of over 1 percent. If a linear voltage ramp is applied to an ideal VCO, a linear-FM waveform is generated. A linear voltage ramp can be generated by applying a voltage step to an analog integrator. The integrator must be reset at the end of the generated pulse. If the VCO has a defined nonlinearity characteristic, the voltage into the integrator can be varied during the pulse so that the voltage ramp compensates for the VCO nonlinearity. Precompensation of this type is often employed. The characteristics of several common VCO devices are given in Table 10.3. The frequency-versus-voltage characteristic of the backward-wave oscillator is exponential; all the others have a linear characteristic. If coherent operation of the VCO is required, the output signal must be phased-locked to a coherent reference signal.

## 10.6 PHASE-CODED WAVEFORMS

---

Phase-coded waveforms differ from FM waveforms in that the pulse is subdivided into a number of subpulses. The subpulses are of equal duration, and each has a particular phase. The phase of each subpulse is selected in accordance with a given code sequence. The most widely used phase-coded waveform employs two phases and is called binary, or biphase, coding. The binary code consists of a sequence of either 0s and 1s or +1s and -1s. The phase of the transmitted signal alternates between  $0^\circ$  and  $180^\circ$  in accordance with the sequence of elements,

**TABLE 10.3** Characteristics of VCO Devices

VCO device	Center-frequency range	Maximum frequency deviation as percent of center frequency, %	Maximum linearity as percent of deviation, %	Maximum center-frequency stability	Comments
LC oscillator	Up to 50 MHz	$\pm 15$	$\pm 0.5$	$\pm 10$ to $\pm 100$ ppm	Requires anode-voltage-control range of 750 to 3000 V. Requires helix-voltage-control range of 400 to 1500 V.
Crystal oscillator	100 kHz to 300 MHz	$\pm 0.25$	$\pm 1$	$\pm 1$ to $\pm 10$ ppm	
Three-terminal gallium arsenide oscillator	60 to 2500 MHz	$\pm 2$	$\pm 2$	$\pm 1\%$	
Voltage-tunable magnetron	100 to 10,000 MHz	$\pm 50$	$\pm 1$	$\pm 0.2\%$	
Backward-wave oscillator	2 to 18 GHz	$\pm 20$	$\pm 0.3^*$	$\pm 0.2\%$	

\*Deviation from an exponential frequency-versus-voltage curve.



0s and 1s or +1s and -1s, in the phase code, as shown in Fig. 10.8. Since the transmitted frequency is not usually a multiple of the reciprocal of the subpulse width, the coded signal is generally discontinuous at the phase-reversal points.

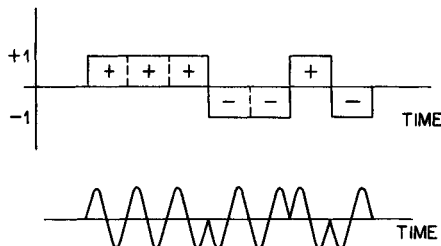


FIG. 10.8 Binary phase-coded signal.

Upon reception, the compressed pulse is obtained by either matched filtering or correlation processing. The width of the compressed pulse at the half-amplitude point is nominally equal to the subpulse width. The range resolution is hence proportional to the time duration of one element of the code. The compression ratio is equal to the number of subpulses in the waveform, i.e., the number of elements in the code.

**Optimal Binary Sequences.** Optimal binary sequences are binary sequences whose peak sidelobe of the aperiodic autocorrelation function (see Fig. 10.10*b* below) is the minimum possible for a given code length. Codes whose autocorrelation function, or zero-doppler responses, exhibit low sidelobes are desirable for pulse compression radars. Responses due to moving targets will differ from the zero-doppler response. However, with proper waveform design the doppler/bandwidth ratio can usually be minimized so that good doppler response is obtained over the target velocities of interest. The range-doppler response, or ambiguity diagram, over this velocity region then approximates the autocorrelation function.

**Barker Codes.** A special class of binary codes is the Barker<sup>21</sup> codes. The peak of the autocorrelation function is  $N$ , and the magnitude of the minimum peak sidelobe is 1, where  $N$  is the number of subpulses or length of the code. Only a small number of these codes exist. All the known Barker codes are listed in Table 10.4 and are the codes which have a minimum peak sidelobe of 1. These codes would be ideal for pulse compression radars if longer lengths were available. However, no Barker codes greater than 13 have been found to exist.<sup>22-24</sup> A pulse compression radar using these Barker codes would be limited to a maximum compression ratio of 13.

**Allomorphic Forms.** A binary code may be represented in any one of four allomorphic forms, all of which have the same correlation characteristics. These forms are the code itself, the inverted code (the code written in reverse order), the complemented code (1s changed to 0s and 0s to 1s), and the inverted complemented code. The number of codes listed in Table 10.4 is the number of codes, not including the allomorphic forms, which have the same minimum peak sidelobe. For example, the following 7-bit Barker codes all have the same

TABLE 10.4 Optimal Binary Codes

Length of code $N$	Magnitude of minimum peak sidelobe	No. of codes	Code (octal notation* for $N > 13$ )
2	1	2	11,10
3	1	1	110
4	1	2	1101,1110
5	1	1	11101
6	2	8	110100
7	1	1	1110010
8	2	16	10110001
9	2	20	110101100
10	2	10	1110011010
11	1	1	11100010010
12	2	32	110100100011
13	1	1	1111100110101
14	2	18	36324
15	2	26	74665
16	2	20	141335
17	2	8	265014
18	2	4	467412
19	2	2	1610445
20	2	6	3731261
21	2	6	5204154
22	3	756	11273014
23	3	1021	32511437
24	3	1716	44650367
25	2	2	163402511
26	3	484	262704136
27	3	774	624213647
28	2	4	1111240347
29	3	561	3061240333
30	3	172	6162500266
31	3	502	16665201630
32	3	844	37233244307
33	3	278	55524037163
34	3	102	144771604524
35	3	222	223352204341
36	3	322	526311337707
37	3	110	1232767305704
38	3	34	2251232160063
39	3	60	4516642774561
40	3	114	14727057244044

\*Each octal digit represents three binary digits:

0	000	4	100
1	001	5	101
2	010	6	110
3	011	7	111

autocorrelation peak value and the same minimum peak sidelobe magnitude: 1110010, 0100111, 0001101, 1011000. For symmetrical codes, the code and its inverse are identical.

*Other Optimal Codes.* Table 10.4 lists the total number of optimal binary codes for all  $N$  up through 40 and gives one of the codes for each  $N$ . As an example, the minimum peak sidelobe for a 19-bit code is 2. There are two codes having this minimum peak sidelobe, one of which is 1610445 = 1 110 001 000 100 100 101. Computer searches are generally used to find optimal codes.<sup>25</sup> However, the search time becomes excessively long as  $N$  increases, and recourse is often made to using other sequences which may not be optimal but possess desirable correlation characteristics.

**Maximal-Length Sequences.** The maximal-length sequences are of particular interest. They are the maximum-length sequences that can be obtained from linear-feedback shift-register generators. They have a structure similar to random sequences and therefore possess desirable autocorrelation functions. They are often called pseudorandom (PR) or pseudonoise (PN) sequences. A typical shift-register generator is shown in Fig. 10.9. The  $n$  stages of the shift register are initially set to all 1s or to combinations of 0s and 1s. The special case of all 0s is not allowed, since this results in an all-zero sequence. The outputs from specific individual stages of the shift register are summed by modulo-2 addition to form the input.

Modulo-2 addition depends only on the number of 1s being added. If the number of 1s is odd, the sum is 1; otherwise, the sum is 0. The shift register is pulsed at the clock-frequency, or shift-frequency, rate. The output of any stage is then a binary sequence. When the feedback connections are properly chosen, the output

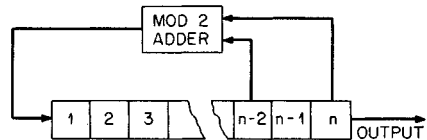


FIG. 10.9 Shift-register generator.

is a sequence of maximal length. This is the maximum length of a sequence of 1s and 0s that can be formed before the sequence is repeated.

The length of the maximal sequence is  $N = 2^n - 1$ , where  $n$  is the number of stages in the shift-register generator. The total number  $M$  of maximum-length sequences that may be obtained from an  $n$ -stage generator is

$$M = \frac{N}{n} \prod \left( 1 - \frac{1}{p_i} \right)$$

where  $p_i$  are the prime factors of  $N$ . The fact that a number of different sequences exist for a given value of  $n$  is important for applications where different sequences of the same length are required.

The feedback connections that provide the maximal-length sequences may be determined from a study of primitive and irreducible polynomials. An extensive list of these polynomials is given by Peterson and Weldon.<sup>26</sup>

Table 10.5 lists the length and number of maximal-length sequences obtainable from shift-register generators consisting of various numbers of stages. A feedback connection for generating one of the maximal-length sequences is also given for each. For a seven-stage generator, the modulo-2 sum of stages 6 and 7 is fed back to the input. For an eight-stage generator, the modulo-2 sum of stages 4, 5, 6, and 8 is fed back to the input. The length  $N$  of the maximal-length sequence is

TABLE 10.5 Maximal-Length Sequences

Number of stages, $n$	Length of maximal sequence, $N$	Number of maximal sequences, $M$	Feedback-stage connections
2	3	1	2,1
3	7	2	3,2
4	15	2	4,3
5	31	6	5,3
6	63	6	6,5
7	127	18	7,6
8	255	16	8,6,5,4
9	511	48	9,5
10	1,023	60	10,7
11	2,047	176	11,9
12	4,095	144	12,11,8,6
13	8,191	630	13,12,10,9
14	16,383	756	14,13,8,4
15	32,767	1,800	15,14
16	65,535	2,048	16,15,13,4
17	131,071	7,710	17,14
18	262,143	7,776	18,11
19	524,287	27,594	19,18,17,14
20	1,048,575	24,000	20,17

equal to the number of subpulses in the sequence and is also equal to the time-bandwidth product of the radar system. Large time-bandwidth products can be obtained from registers having a small number of stages. The bandwidth of the system is determined by the clock rate. Changing both the clock rate and the feedback connections permits the generation of waveforms of various pulse lengths, bandwidths, and time-bandwidth products. The number of zero crossings, i.e., transitions from 1 to 0 or from 0 to 1, in a maximal-length sequence is  $2^{n-1}$ .

Periodic waveforms are obtained when the shift-register generator is left in continuous operation. They are sometimes used in CW radars. Aperiodic waveforms are obtained when the generator output is truncated after one complete sequence. They are often used in pulsed radars. The autocorrelation functions for these two cases differ with respect to the sidelobe structure. Figure 10.10 gives the autocorrelation functions for the periodic and aperiodic cases for a typical 15-element maximal-length code obtained from a four-stage shift-register generator. The sidelobe level for the periodic case is constant at a value of  $-1$ . The periodic autocorrelation function is repetitive with a period of  $N\tau$  and

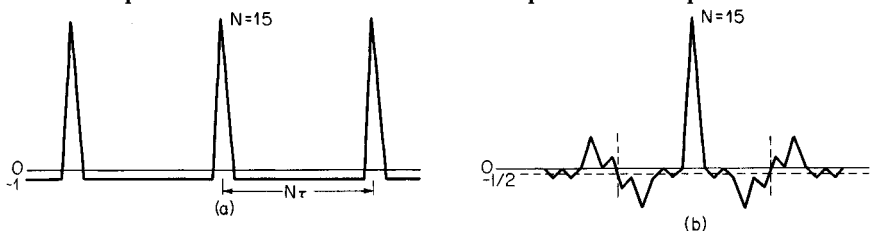


FIG. 10.10 Autocorrelation functions for (a) the periodic case and (b) the aperiodic case.

a peak value of  $N$ , where  $N$  is the number of subpulses in the sequence and  $\tau$  is the time duration of each subpulse. Hence the peak-sidelobe-voltage ratio is  $N^{-1}$ .

For the aperiodic case, the average sidelobe level along the time axis is  $-1/2$ . The sidelobe structure of each half of the autocorrelation function has odd symmetry about this value. The periodic autocorrelation function may be viewed as being constructed by the superposition of successive aperiodic autocorrelation functions, each displaced in time by  $N\tau$  units. The odd symmetry exhibited by the aperiodic function causes the sidelobe structure for the periodic function to have a constant value of  $-1$ . When the periodic waveform is truncated to one complete sequence, this constant sidelobe property is destroyed. For large  $N$  the peak-sidelobe-voltage ratio is approximately  $N^{-1/2}$  for the aperiodic case.

Maximal-length sequences have characteristics which approach the three randomness characteristics ascribed to truly random sequences,<sup>27</sup> namely, that (1) the number of 1s is approximately equal to the number of 0s; (2) runs of consecutive 1s and 0s occur with about half of the runs having a length of 1, a quarter of length 2, an eighth of length 3, etc.; and (3) the autocorrelation function is thumbtack in nature, i.e., peaked at the center and approaching zero elsewhere. Maximal-length sequences are of odd length. In many radar systems it is desirable to use sequence lengths of some power of 2. A common procedure is to insert an extra 0 in a maximal-length sequence. This degrades the autocorrelation function sidelobes somewhat. An examination of sequences with an inserted 0 will yield the sequence with the best autocorrelation characteristics.

**Quadratic Residue Sequences.** Quadratic residue (p. 254 of Ref. 26), or Legendre, sequences offer a greater selection of code lengths than are available from maximal-length sequences. Quadratic residue sequences satisfy two of the randomness characteristics: the periodic autocorrelation function is as shown in Fig. 10.10a having a peak of  $N$  and a uniform sidelobe level of  $-1$ , and the number of 1s is approximately the same as the number of 0s.

A quadratic residue sequence of length  $N$  exists if  $N = 4t - 1$ , with  $N$  a prime and  $t$  any integer. The code elements  $a_i$  for  $i = 0, 1, 2, \dots, N - 1$  are 1 if  $i$  is a quadratic residue modulo  $N$  and  $-1$  otherwise. Quadratic residues are the remainders where  $x^2$  is reduced modulo  $N$  for  $x = 1, 2, \dots, (N - 1)/2$ . As an example, the quadratic residues for  $N = 11$  are 1, 3, 4, 5, 9. Hence the code elements  $a_i$  for  $i = 1, 3, 4, 5, 9$  are 1, and the sequence is  $-1, 1, -1, 1, 1, 1, -1, -1, -1, 1, -1$ , or 10100011101. The periodic autocorrelation function of this sequence has a peak of 11 and a uniform sidelobe level of  $-1$ . Also, the numbers of 1s and 0s are approximately equal; the number of 1s is one more than the number of 0s.

**Complementary Sequences.** Complementary sequences consist of two sequences of the same length  $N$  whose aperiodic autocorrelation functions have sidelobes equal in magnitude but opposite in sign. The sum of the two autocorrelation functions has a peak of  $2N$  and a sidelobe level of zero. Figure 10.11 shows the individual autocorrelation functions of the complementary sequences for length 26 and also the sum of the two autocorrelation functions. Golay<sup>28,29</sup> and Hollis<sup>30</sup> discuss general methods for forming complementary codes. In general,  $N$  must be an even number and the sum of two squares. In a practical application, the two sequences must be separated in time, frequency, or polarization, which results in decorrelation of radar returns so that complete sidelobe cancellation may not occur. Hence they have not been widely used in pulse compression radars.

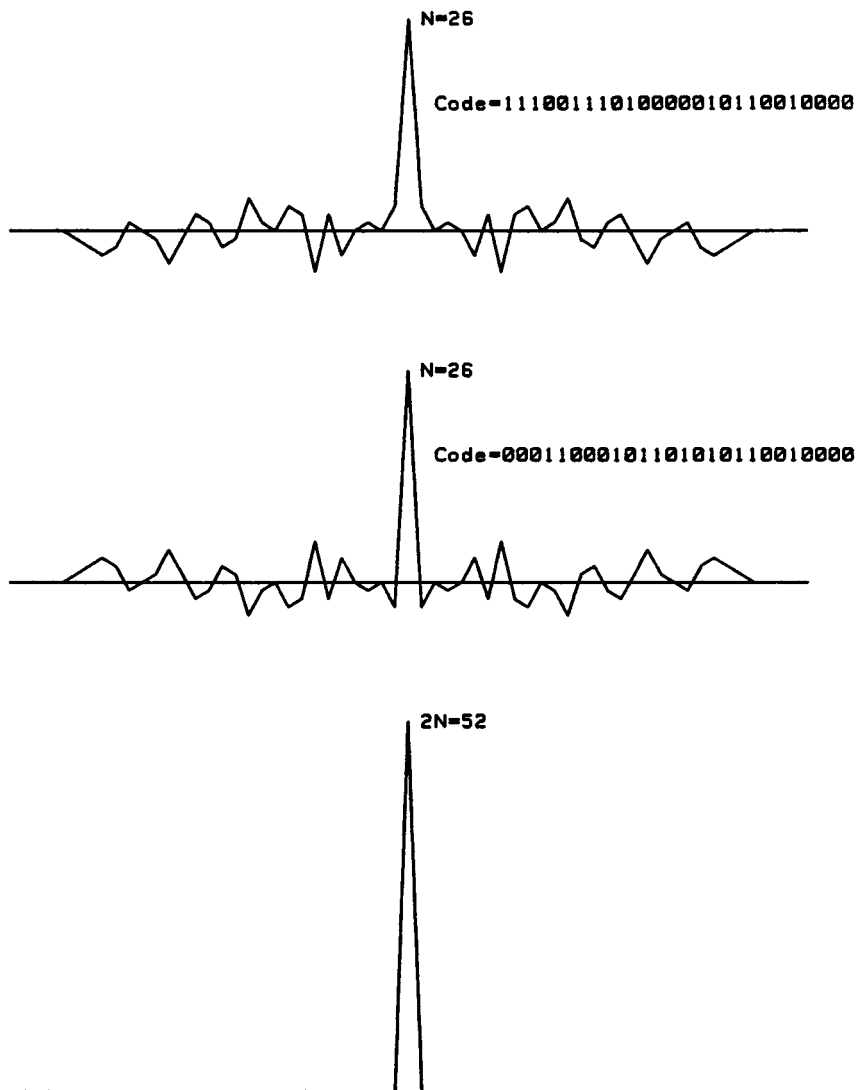


FIG. 10.11 Complementary-code aperiodic autocorrelation function.

**Implementation of Biphase-Coded Systems.** Digital implementation is generally used to perform the pulse compression operation in biphase-coded systems. A block diagram of a digital pulse compression system is given in Fig. 10.12. The code generator generates the binary sequence, which is sent to the RF modulator and transmitter and to the correlators. Received IF signals are passed through a bandpass filter matched to the subpulse width and are demodulated by  $I$  and  $Q$  phase detectors. The  $I$  and  $Q$  detectors compare the phase of the received IF signal with the phase of a local-oscillator (LO) signal at the same IF frequency. The LO signal is also used in the RF modulator to

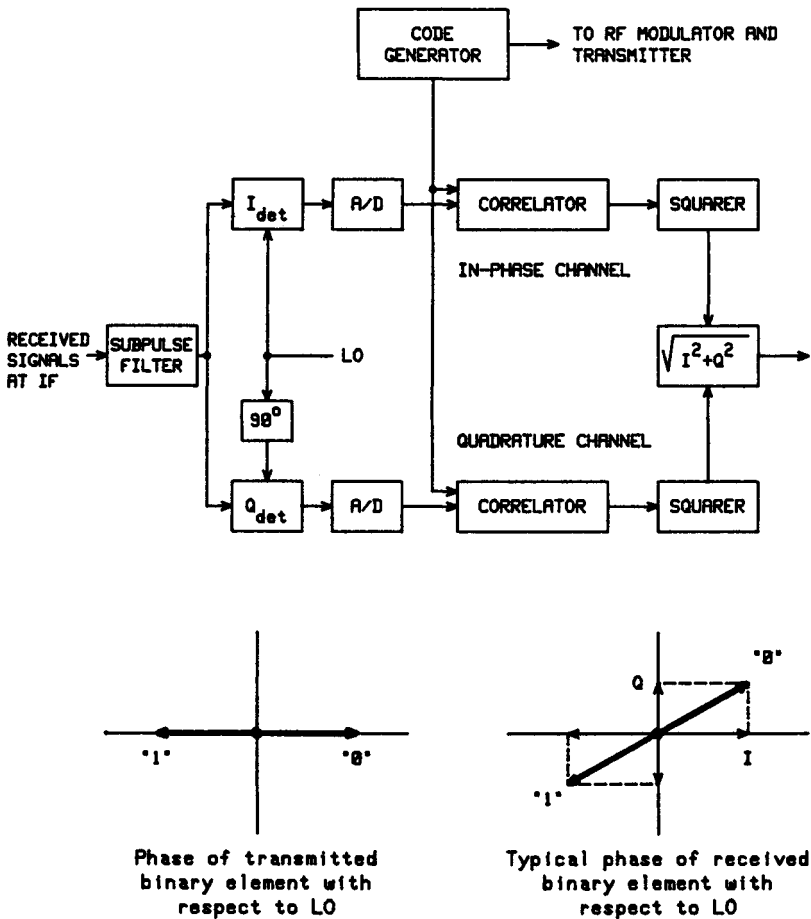


FIG. 10.12 Digital pulse compression for phase-coded signals.

generate the biphas-modulated transmitted signal. The phase of each transmitted binary element is  $0^\circ$  or  $180^\circ$  with respect to the LO signal. The phase of the received signal with respect to the LO signal, however, is shifted by an amount depending upon the target's range and velocity. Two processing channels are used, one which recovers the in-phase components of the received signal and the other which recovers the quadrature components. These signals are converted to digital form by analog-to-digital (A/D) converters, correlated with the stored binary sequence and combined, e.g., by the square root of the sum of the squares. A processing system of this type, which contains an in-phase and quadrature channel and two matched filters or correlators, is called a homodyne or zero IF system. There is an average loss in signal-to-noise ratio of 3 dB if only one channel is implemented instead of both  $I$  and  $Q$  channels. Each correlator may actually consist of several correlators, one for each quantization bit of the digitized signal.

Two methods of implementing the correlators are shown in Fig. 10.13. Fig-

ure 10.13a shows a fixed reference correlator; i.e., only one binary sequence is used. The received input sequence is continuously clocked into a shift register whose number of stages is equal to the number of elements in the sequence. The output of each stage is multiplied by weight  $a_i$ , which is either +1 or -1 in accordance with the reference sequence. The summation circuit provides the output correlation function or compressed pulse.

Figure 10.13b shows an implementation where the reference may be changed for each transmitted pulse. The transmitted reference sequence is fed into the reference shift register. The received input sequence is continuously clocked into the signal shift register. In each clock period the comparison counter forms the sum of the matches minus the sum of the mismatches between corresponding stages of the two shift registers, which is the output correlation function. In some systems, only the sum of the matches is counted and an offset of  $-N/2$  is added to the sum.

**Doppler Correction.** In many applications the effect of doppler is negligible over the expanded pulse length, and no doppler correction or compensation is required. These applications transmit a short-duration phase-coded pulse, and

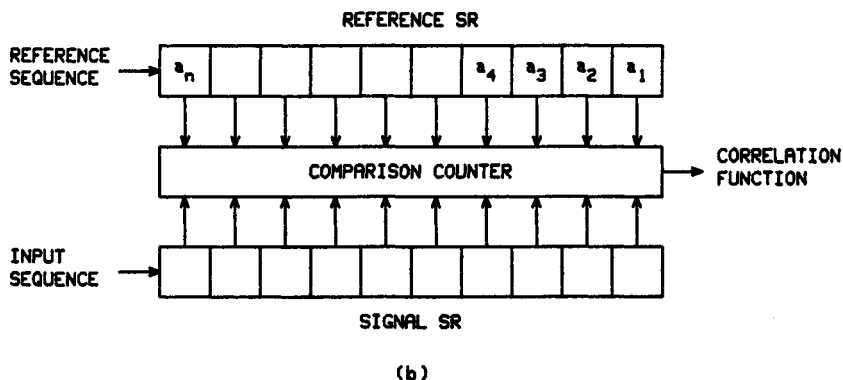
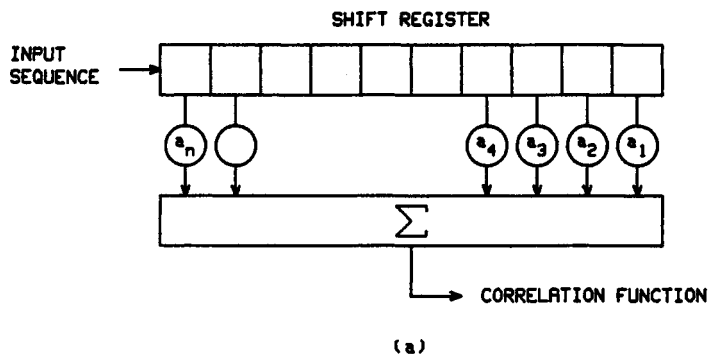


FIG. 10.13 Digital correlation with (a) fixed and (b) variable references.



the phase shift due to doppler over each expanded pulse width is negligible. Pulse compression is performed on each pulse. When the doppler shift over the expanded pulse width is not negligible, multiple doppler channels are required to minimize the loss in SNR. The received signals may be mixed with multiple LO signals (see Fig. 10.12), each offset in frequency by an amount corresponding to a doppler resolution element which is the reciprocal of the expanded pulse length. The processing following the subpulse filter in Fig. 10.12 is then duplicated for each doppler channel.

An alternative technique is to use a single LO signal and single-bit A/D converters in Fig. 10.12. Doppler compensation is performed on the outputs of the A/D converters prior to the correlators. This doppler compensation is in the form of inverting data bits, i.e., changing 1s to 0s and 0s to 1s, at time intervals corresponding to  $180^\circ$  phase shifts of the doppler frequency. As an example, the first doppler channel corresponds to a doppler frequency which results in a  $360^\circ$  phase shift over the pulse width. The bits are inverted after every half pulse width and remain inverted for a half pulse width. Bit inversion occurs at intervals of a quarter pulse width for the second doppler channel, an eighth pulse width for the third doppler channel, etc. Negative doppler frequency channels are handled in the same manner as for positive doppler frequency channels, but bits that were inverted in the corresponding positive channel are not inverted in the negative channel, and bits that were not inverted in the positive channel are inverted in the negative channel. No bit inversion occurs in the zero doppler channel. Each doppler channel consists of the single-bit  $I$  and  $Q$  correlators and the combiner, e.g., square root of the sum of the squares. After initial detection occurs, linear doppler processing may then be used to reduce the SNR loss. For example, the LO signal in Fig. 10.12 would then correspond to the doppler which resulted in the initial detection, and full A/D conversion is used. Some radar systems use long-duration pulses with single-bit doppler compensation to obtain initial detection and then switch to shorter-duration pulses which require no doppler compensation.

**Polyphase Codes.** Waveforms consisting of more than two phases may also be used.<sup>31,32</sup> The phases of the subpulses alternate among multiple values rather than just the  $0^\circ$  and  $180^\circ$  of binary phase codes. The Frank polyphase codes<sup>33</sup> derive the sequence of phases for the subpulses by using a matrix technique. The phase sequence can be written as  $\phi_n = 2\pi i(n-1)/P^2$ , where  $P$  is the number of phases,  $n = 0, 1, 2, \dots, P^2 - 1$ , and  $i = n$  modulo  $P$ . For a three-phase code,  $P = 3$ , and the sequence is  $0, 0, 0, 0, 2\pi/3, 4\pi/3, 0, 4\pi/3, 2\pi/3$ .

The autocorrelation function for the periodic sequence has time sidelobes of zero. For the aperiodic sequence, the time sidelobes are greater than zero. As  $P$  increases, the peak-sidelobe-voltage ratio approaches  $(\pi P)^{-1}$ . This corresponds to approximately a 10 dB improvement over pseudorandom sequences of similar length. The ambiguity response over the range-doppler plane grossly resembles the ridgelike characteristics associated with linear-FM waveforms, as contrasted with the thumbtack characteristic of pseudorandom sequences. However, for small ratios of doppler frequency to radar bandwidth, good doppler response can be obtained for reasonable target velocities.

Lewis and Kretschmer<sup>34</sup> have rearranged the phase sequence to reduce the degradation that may occur by receiver band limiting prior to pulse compression. The rearranged phase sequence is

$$\phi_n = \frac{n\pi}{P} \left[ 1 - P + \frac{2(n-i)}{P} \right] \quad \text{for } P \text{ odd}$$

$$\phi_n = \frac{\pi}{2P}(P - 1 - 2i) \left[ P - 1 - \frac{2(n - i)}{P} \right] \quad \text{for } P \text{ even}$$

where  $P$ ,  $n$ , and  $i$  are as defined above for the Frank code. For  $P = 3$ , the phase sequence is  $0, -2\pi/3, -4\pi/3, 0, 0, 0, 2\pi/3, 4\pi/3$ .

Generation and processing of polyphase waveforms use techniques similar to those for the FM waveforms of Sec. 10.5.

## 10.7 TIME-FREQUENCY-CODED WAVEFORMS

A time-frequency-coded waveform (Fig. 10.14) consists of a train of  $N$  pulses with each pulse transmitted at a different frequency. The ambiguity response for a periodic waveform of this type consists of a central spike plus multiple spikes or ridges displaced in time and frequency. The objective is to create a high-resolution, thumbtacklike central spike with a clear area around it; measurement is then performed on the high-resolution central spike. The range resolution or compressed pulse width is determined by the total bandwidth of all the pulses, and the doppler resolution is determined by the waveform duration  $T$ . For example, a typical waveform in this class has  $N$  contiguous pulses of width  $\tau$ , whose spectra of width  $1/\tau$  are placed side by side in frequency to eliminate gaps in the composite spectrum. Since the waveform bandwidth is now  $N/\tau$ , the nominal compressed-pulse width is  $\tau/N$ . Relationships are summarized in Table 10.6.

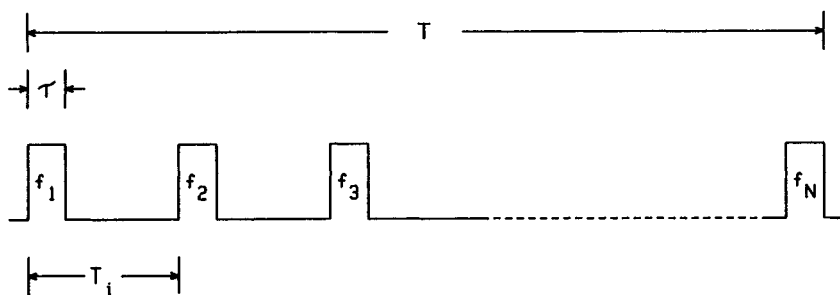


FIG. 10.14 Time-frequency-coded waveform.

TABLE 10.6  $N$  Pulses Contiguous in Time and Frequency

Waveform duration, $T$	$N\tau$
Waveform bandwidth, $B$	$N/\tau$
Time-bandwidth product, $TB$	$N^2$
Compressed pulse width, $1/B$	$\tau/N = T/N^2$

Shaping of the high-resolution central spike area as well as the gross structure of the ambiguity surface can be accomplished by variations of the basic waveform parameters such as amplitude weighting of the pulse train, staggering

of the pulse repetition interval, and frequency or phase coding of the individual pulses.<sup>35</sup>

## 10.8 WEIGHTING AND EQUALIZATION

The process of shaping the compressed-pulse waveform by adjustment of the amplitude of the frequency spectrum is known as *frequency weighting*. The process of shaping the doppler response by control of the waveform envelope shape is called *time weighting*. The primary objective of weighting in either domain is to reduce sidelobes in the other domain. Sidelobes can severely limit resolution when the relative magnitudes of received signals are large.

**Paired Echoes and Weighting.** A description of the weighting process is facilitated by the application of paired-echo theory.<sup>36-39</sup> The first seven entries in Table 10.7 provide a step-by-step development of Fourier transforms useful in frequency and time weighting, starting with a basic transform pair. The last entry pertains to phase-distortion echoes. The spectrum  $G(f)$  of the time function  $g(t)$  is assumed to have negligible energy outside the frequency interval  $-B/2$  to  $+B/2$ , where  $B$  is the bandwidth in hertz. The transform pairs of Table 10.7 are interpreted as follows:

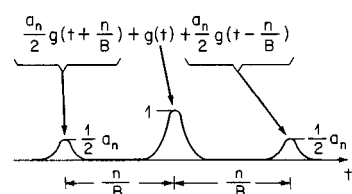
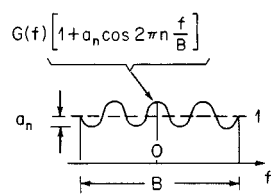
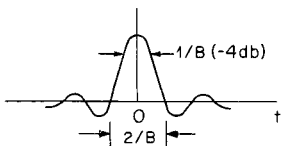
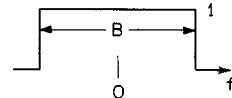
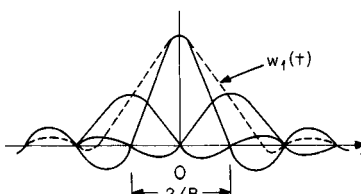
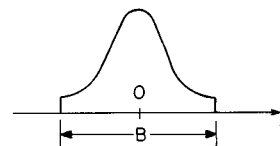
**Pair 1.** Cosinusoidal amplitude variation over the passband creates symmetrical paired echoes in the time domain in addition to the main signal  $g(t)$ , whose shape is uniquely determined by  $G(f)$ . The echoes are replicas of the main signal, delayed and advanced from it by  $n/B$  s and scaled in amplitude by  $a_n/2$ .

**Pair 2.** The rectangular frequency function  $W_0(f)$ , that is, uniform weighting over the band, leads to a  $(\sin x)/x$  time function  $w_0(t)$  with high-level sidelobes, which can be objectionable in some cases. A normalized logarithmic plot of the magnitude of this time function is shown by curve *A* in Fig. 10.15. (All functions illustrated are symmetrical about  $t = 0$ .) The sidelobe adjacent to the main lobe has a magnitude of  $-13.2$  dB with respect to the main-lobe peak. The sidelobe falloff rate is very slow.

**Pair 3.** Taper is applied by introducing one amplitude ripple ( $n = 1$ ) in the frequency domain to form  $W_1(f)$ . By pairs 1 and 2, the time function is the superposition of the three time-displaced and weighted  $(\sin x)/x$  functions.<sup>39</sup> Low time sidelobes are attainable in the resultant function  $w_1(t)$  by the proper choice of the coefficient  $F_1$ . In particular,  $F_1 = 0.426$  corresponds to Hamming weighting<sup>40-42</sup> and to the time function whose magnitude is represented by the solid curve *B* in Fig. 10.15.

**Pair 4.** The frequency-weighting function includes a Fourier series of  $\bar{n} - 1$  cosine terms, where the selection of  $\bar{n}$  is determined by the required compressed pulse width and the desired sidelobe falloff. By pairs 1 and 2, the time function includes the superposition of  $2(\bar{n} - 1)$  echoes that occur in  $\bar{n} - 1$  symmetrical pairs. If the coefficients  $F_m$  are selected to specify the Taylor weighting function<sup>39,42,43</sup>  $W_{\text{Tay}}(f)$ , the corresponding resultant time function  $w_{\text{Tay}}(t)$  exhibits good resolution characteristics by the criterion of small main-lobe width for a specified sidelobe level. Taylor coefficients chosen for a  $-40$  dB sidelobe level, with  $\bar{n}$  selected as 6, lead to the main-sidelobe structure indicated by curve *C* of Fig. 10.15.

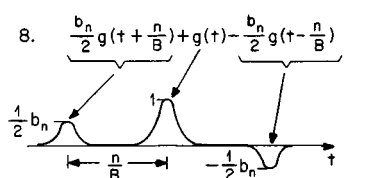
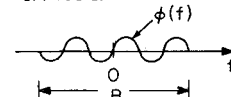
TABLE 10.7 Paired-Echo and Weighting Transforms

$g(t) = \int_{-\infty}^{\infty} G(f) \exp(j2\pi ft) df$	$G(f) = \int_{-\infty}^{\infty} g(t) \exp(-j2\pi ft) dt$
<p><u>PAIRED ECHOES:</u></p> <p>1. <math>\frac{a_n}{2} g(t + \frac{n}{B}) + g(t) + \frac{a_n}{2} g(t - \frac{n}{B})</math></p> 	<p><u>n AMPLITUDE RIPPLES:</u></p> <p><math>G(f) \left[ 1 + a_n \cos 2\pi n \frac{f}{B} \right]</math></p>  <p style="text-align: right;">(REFS. 36-39)</p>
<p><u>HIGH SIDELOBES (-13.2 db):</u></p> <p>2. <math>w_0(t) = B \frac{\sin \pi B t}{\pi B t}</math></p> 	<p><u>UNIFORM WEIGHTING:</u></p> <p><math>w_0(f) = \begin{cases} 1 &amp;  f  &lt; \frac{1}{2} B \\ 0 &amp;  f  &gt; \frac{1}{2} B \end{cases}</math></p> 
<p><u>LOW SIDELOBES:</u></p> <p>3. <math>w_1(t) = F_1 w_0(t + \frac{1}{B}) + w_0(t) + F_1 w_0(t - \frac{1}{B})</math></p> 	<p><u>TAPER:</u></p> <p><math>w_1(f) = W_0(f) \left[ 1 + 2F_1 \cos 2\pi \frac{f}{B} \right]</math></p>  <p style="text-align: right;">(REFS. 39-42)</p>

**Pairs 5 to 7.** The duality theorem 5 permits the interchange of time and frequency functions in each of the preceding pairs. Functions may be interchanged if the sign of the parameter  $t$  is reversed. Examples are pairs 6 and 7 obtainable from pairs 2 and 4 with the substitution of  $T$  s for  $B$  Hz. Taylor time weighting is applied in pair 7 to achieve good frequency resolution when the coefficients are selected for a specified sidelobe level.

**Pair 8.** Similarly to the amplitude variations of pair 1, sinusoidal phase variation over the passband creates symmetrical paired echoes in the time domain in addition to the main signal  $g(t)$ . The echoes are replicas of the main signal, de-

**TABLE 10.7** Paired-Echo and Weighting Transforms (*Continued*)

<p>4. <math>w_{\text{Tay}}(t) = \sum_{m=-\infty}^{\infty} F_m w_0(t - \frac{m}{B})</math></p> <p>where  <math>F_0 = 1, F_m = 0</math> for <math> m  \geq \bar{n}</math>                      and  <math>F_m = E_m</math></p>	<p><u>TAYLOR WEIGHTING:</u></p> <p><math>W_{\text{Tay}}(f) =</math>  <math>W_0(f) \left[ 1 + 2 \sum_{m=1}^{\bar{n}-1} F_m \cos 2\pi m \frac{f}{B} \right]</math></p> <p>(REFS. 39,42,43)</p>
<p><u>DUALITY THEOREM:</u></p> <p>5. <math>G(-t)</math></p>	<p><math>g(f)</math></p>
<p>6. <math>W_0(t) = \begin{cases} 1 &amp;  t  &lt; \frac{T}{2} \\ 0 &amp;  t  &gt; \frac{T}{2} \end{cases}</math></p>	<p><math>w_0(f) = T \frac{\sin \pi f T}{\pi f T}</math></p>
<p>7. <math>W_{\text{Tay}}(t) =</math>  <math>W_0(t) \left[ 1 + 2 \sum_{m=1}^{\bar{n}-1} F_m \cos 2\pi m \frac{t}{T} \right]</math></p>	<p><math>w_{\text{Tay}}(f) = \sum_{m=-\infty}^{\infty} F_m w_0(f - \frac{m}{T})</math></p> <p>(SEE PAIR No. 4)</p>
<p><u>PAIRED ECHOES:</u></p> <p>8. <math>\frac{b_n}{2} g(t + \frac{n}{B}) + g(t) - \frac{b_n}{2} g(t - \frac{n}{B})</math></p> 	<p><u>n PHASE RIPPLES:</u></p> <p><math>G(f) e^{j b_n \sin 2\pi n \frac{f}{B}} \cong</math>  <math>\left[ 1 + j b_n \sin 2\pi n \frac{f}{B} \right] G(f)</math></p> <p><math> b_n  &lt; 0.4</math> radian</p>  <p>(REFS. 36-39)</p>

layed and advanced from it by  $n/B$  s, scaled in amplitude by  $b_n/2$ , and opposite in polarity.

**Comparison of Weighting Functions.** The performance achieved with various frequency-weighting functions is summarized in Table 10.8. With a change in parameter, the table also applies to time weighting (or weighting of the aperture distribution of an antenna). Pedestal height  $H$  is defined in all cases as the weighting-function amplitude at the band edge ( $f = \pm B/2$ ) when the function has been normalized to unit amplitude at the band center ( $f = 0$ ). The loss in the signal-to-noise ratio is based on the assumption that the transmitted amplitude spectrum is rectangular.

Item 1, uniform weighting, thus provides matched-filter operation with no

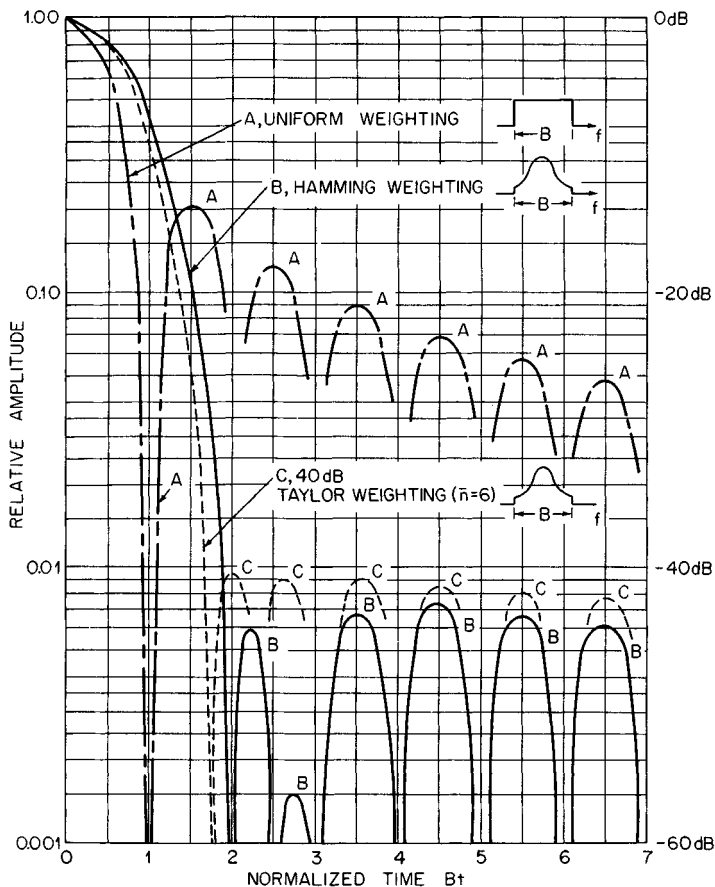


**FIG. 10.15** Comparison of compressed-pulse shapes for three frequency-weighting functions.

SNR loss. Weighting in other cases is applied by a mismatch of the receiver amplitude characteristic. Item 2, Dolph-Chebyshev<sup>44</sup> weighting, is optimum in the sense of producing the minimum main-lobe width for a specified sidelobe level. However, the Dolph-Chebyshev function is physically unrealizable<sup>39,41,42</sup> for the continuous spectra under discussion. Item 3, Taylor weighting, provides a realizable approximation to Dolph-Chebyshev weighting. Time sidelobes have little decay in the region  $B|t| \ll \bar{n} - 1$  but decay at 6 dB per octave when  $B|t| \gg \bar{n}$ . Item 4, cosine-squared-plus-pedestal weighting, becomes equivalent, after normalization and use of a trigonometric identity, to the weighting function  $W_1(f)$  of pair 3 in Table 10.7. The normalized pedestal height  $H$  is related to the taper coefficient  $F_1$  by  $H = (1 - 2F_1)/(1 + 2F_1)$ . The Hamming function produces the lowest sidelobe level attainable under category 4 of Table 10.8. Item 4b, 3:1 taper ratio (that is,  $1/H = 3$ ), is analogous to a typical antenna distribution with power tapering to about 10 percent at the aperture edges.<sup>45</sup> Cosine-squared weighting without pedestal

TABLE 10.8 Performance for Various Frequency-Weighting Functions

	Weighting function	Pedestal height $H$ , %	SNR loss, dB	Main-lobe width, -3 dB	Peak sidelobe level, dB	Far sidelobe falloff
1	Uniform	100	0	$0.886/B$	-13.2	6 dB/octave
2	Dolph-Chebyshev			$1.2/B$	-40	No decay
3	Taylor ( $\bar{n} = 8$ )	11	1.14	$1.25/B$	-40	6 dB*/octave
4	Cosine-squared plus pedestal: $H + (1 - H) \cos^2(\pi f/B)$					
	a. Hamming	8	1.34	$1.33/B$	-42.8	6 dB/octave
	b. 3:1 "taper ratio"	33.3	0.55	$1.09/B$	-25.7	6 dB/octave
5	$\cos^2(\pi f/B)$	0	1.76	$1.46/B$	-31.7	18 dB/octave
6	$\cos^3(\pi f/B)$	0	2.38	$1.66/B$	-39.1	24 dB/octave
7	$\cos^4(\pi f/B)$	0	2.88	$1.94/B$	-47	30 dB/octave
8	Triangular: $1 - 2 f /B$	0	1.25	$1.27/B$	-26.4	12 dB/octave

\*In the region  $|f| \approx 8/B$ .

( $H = 0$ ,  $F_1 = 1/2$ ), listed as item 5, achieves a faster decay in far-off sidelobes and may simplify implementation. Entries 6 to 8 are of interest primarily because of the sidelobe falloff rate. The falloff rate can be shown to be related to the manner in which the frequency function and its derivatives behave at cut-off points,  $f = \pm B/2$ .<sup>46,47</sup>

**Taylor versus Cosine-Squared-Plus-Pedestal Weighting.** Figure 10.16a plots the taper coefficient  $F_1$  and pedestal height  $H$  versus the peak sidelobe level for cosine-squared-plus-pedestal weighting. Table 10.9 lists Taylor coefficients  $F_m$  and main-lobe widths for various sidelobe levels and selections of  $\bar{n}$ .<sup>48</sup> The table illustrates that, for low design sidelobe levels,  $F_1$  is much greater than  $|F_m|$  when  $m > 1$ , indicating that Taylor weighting is closely approximated by the cosine-squared-plus-pedestal taper. A larger value of  $F_1$  is required, however, in the latter case to yield the same sidelobe level.  $F_1 = 0.426$  ( $H = 0.08$ ), corresponding to Hamming weighting, produces the lowest level, -42.8 dB, attainable with this function. As indicated in Fig. 10.16a, larger values of  $F_1$  ( $H < 0.08$ ) increase the sidelobe level. For a given peak sidelobe level, Taylor weighting offers theoretical advantages in pulse width and SNR performance, as illustrated in Fig. 10.16b and c.

**Taylor Weighting with Linear FM.** The spectrum of a linear-FM pulse with a rectangular time envelope is not exactly rectangular in amplitude, nor is its phase exactly matched by the linear group delay of the compression filter.<sup>2,39,42</sup> The discrepancy is particularly severe for small time-bandwidth products. Therefore, the use of 40 dB Taylor weighting based on a simplified model which assumes a rectangular amplitude spectrum and a parabolic phase spectrum (that can be matched by the linear group delay) fails to achieve a -40 dB sidelobe level. Further degradation results when there is a doppler shift. Figure 10.17 plots the peak sidelobe level versus the target's doppler

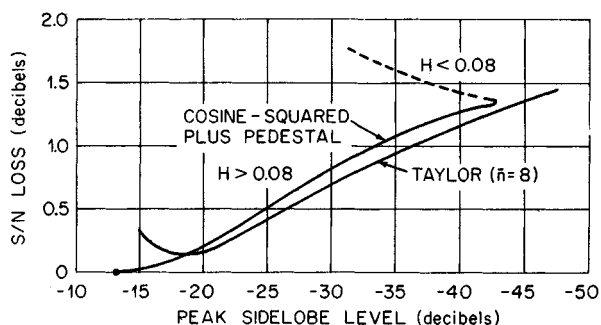
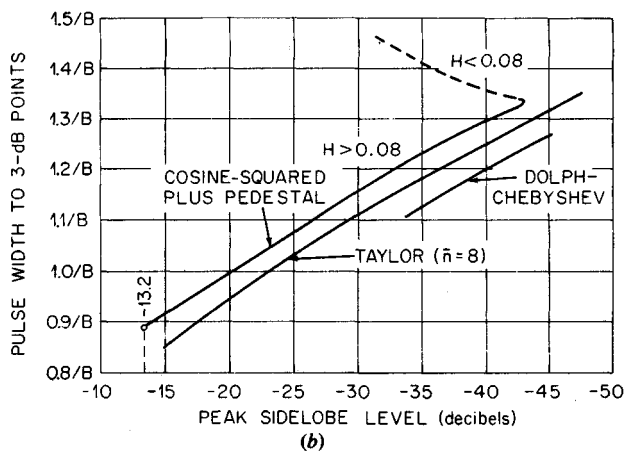
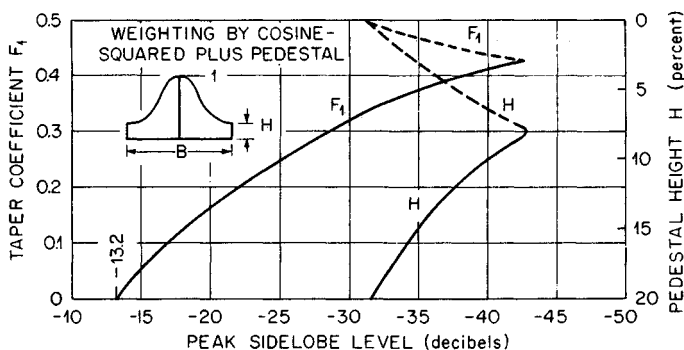


**FIG. 10.16** (a) Taper coefficient and pedestal height versus peak sidelobe level. (b) Compressed-pulse width versus peak sidelobe level. (c) SNR loss versus peak sidelobe level.



TABLE 10.9 Taylor Coefficients  $F_m^*$ 

Design sidelobe ratio, dB	-30	-35	-40	-40	-45	-45	-50
$\bar{n}$	4	5	6	8	8	10	10
Main lobe width, -3 dB	$1.13/B$	$1.19/B$	$1.25/B$	$1.25/B$	$1.31/B$	$1.31/B$	$1.36/B$
$F_1$	0.292656	0.344350	0.389116	0.387560	0.428251	0.426796	0.462719
$F_2$	-0.157838(-1)	-0.151949(-1)	-0.945245(-2)	-0.954603(-2)	0.208399(-3)	-0.682067(-4)	0.126816(-1)
$F_3$	0.218104(-2)	0.427831(-2)	0.488172(-2)	0.470359(-2)	0.427022(-2)	0.420099(-2)	0.302744(-2)
$F_4$		-0.734551(-3)	-0.161019(-2)	-0.135350(-2)	-0.193234(-2)	-0.179997(-2)	-0.178566(-2)
$F_5$			0.347037(-3)	0.332979(-4)	0.740559(-3)	0.569438(-3)	0.884107(-3)
$F_6$				0.357716(-3)	-0.198534(-3)	0.380378(-5)	-0.382432(-3)
$F_7$				-0.290474(-3)	0.339759(-5)	-0.224597(-3)	0.121447(-3)
$F_8$						0.246265(-3)	-0.417574(-5)
$F_9$						-0.153486(-3)	-0.249574(-4)

\* $F_0 = 1$ ;  $F_{-m} = F_m$ ; floating decimal notation:  $-0.945245(-2) = -0.00945245$ .

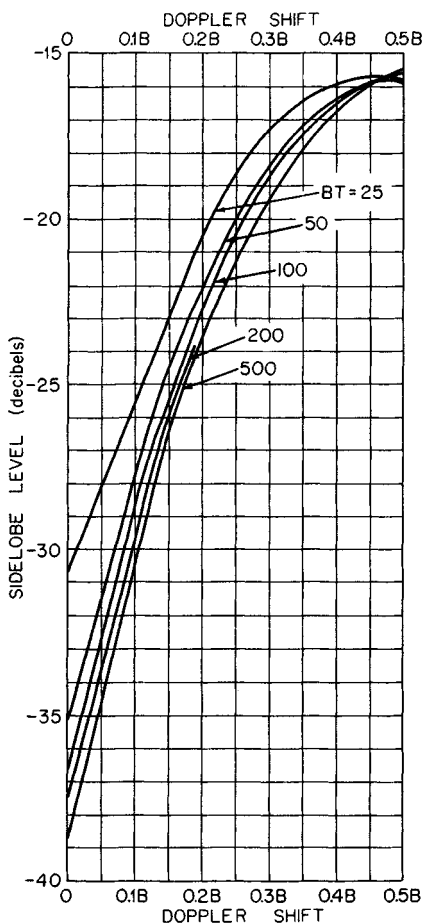


FIG. 10.17 Peak sidelobe level versus doppler shift for linear FM.

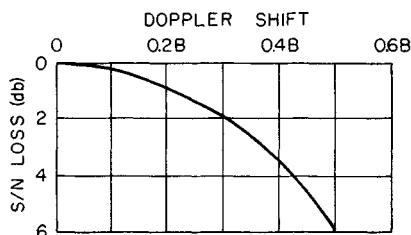


FIG. 10.18 Loss in signal-to-noise ratio versus doppler shift for linear FM.

frequency. As the time-bandwidth product is increased, the model rectangular spectrum with parabolic phase is approached, and the sidelobe level in the absence of doppler shift approaches  $-40$  dB. Unless SAW compression networks that compensate for the nonideal spectrum are employed, equalization techniques described later in this section are needed when sidelobe levels lower than about  $-30$  dB are required. In Fig. 10.18 the loss in signal-to-noise ratio is plotted as a function of doppler shift. To obtain the total SNR loss with respect to that achieved with matched-filter reception, it is necessary to add 1.15 dB (see Fig. 10.16c for Taylor weighting) to the loss of Fig. 10.18.

**Discrete Time Weighting<sup>2</sup>.** A stepped-amplitude function for the reduction of doppler sidelobes is shown in Fig. 10.19. It is symmetrical about the origin, with  $N$  denoting the number of steps on each side. Table 10.10 lists stepped-amplitude functions optimized to yield minimum peak sidelobes for  $N = 2, 3, 4,$  and  $5$ .  $N = 1$ , corresponding to the rectangular time envelope, is included for comparison. For  $N = 2, 3,$  and  $4$ , the list corresponds very closely to stepped-antenna-aperture distributions<sup>49</sup> optimized by the criterion of maximizing the percentage energy included between the first nulls of the antenna radiation pattern.

**Amplitude and Phase Distortion.** The ideal compressed pulse has an amplitude spectrum that exactly matches the frequency-weighting function chosen to meet time-sidelobe requirements. Its phase spectrum is linear, corresponding to constant group delay over the band. Amplitude and phase distortion represent a departure of the actual spectrum from this ideal. All radar components are potential sources of distortion which can

**TABLE 10.10** Optimum Stepped-Amplitude Time-Weighting Functions

$N$	Peak sidelobe, dB	Main-lobe width, -3 dB	$a_1$	$a_2$	$a_3$	$a_4$	$a_5$	$b_1$	$b_2$	$b_3$	$b_4$	$b_5$
1	-13.2	$0.886/T$	1					1				
2	-20.9	$1.02/T$	0.5	0.5				1	0.55			
3	-23.7	$1.08/T$	0.35	0.35	0.30			1	0.625	0.350		
4	-27.6	$1.14/T$	0.25	0.25	0.25	0.25		1	0.78	0.56	0.34	
5	-29.6	$1.16/T$	0.300	0.225	0.235	0.170	0.070	1	0.72	0.54	0.36	0.18

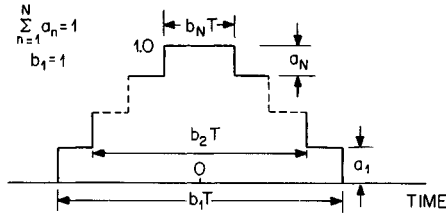


**FIG. 10.19** Stepped-amplitude time weighting.

contribute to cumulative radar system distortion. Distortion degrades system performance usually by increasing the sidelobe level and, in extreme cases, by reducing the SNR and increasing the pulse width.

The paired-echo concept is useful in estimating distortion tolerances necessary to achieve a required time-sidelobe level.<sup>50</sup> Pair 1 of Table 10.7 shows

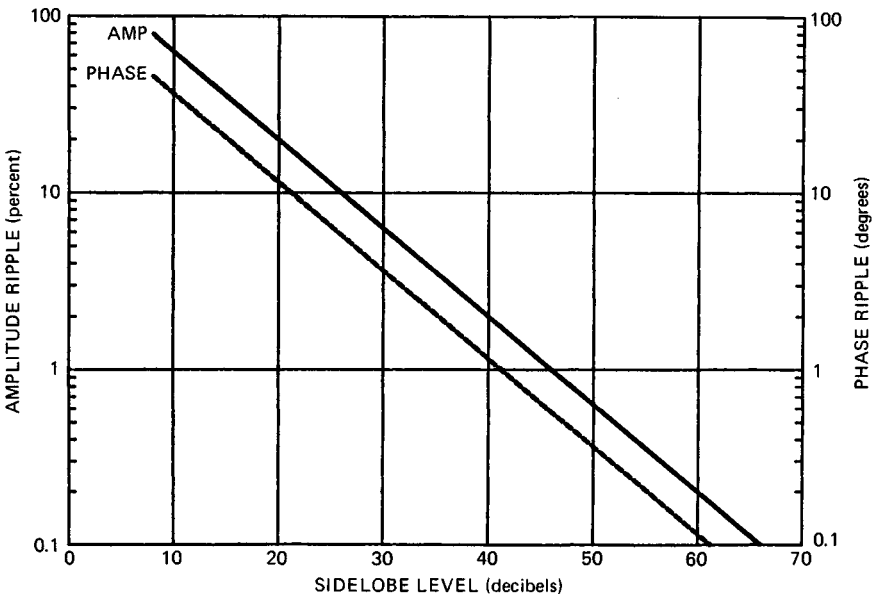


**FIG. 10.20** Distortion tolerances versus time sidelobes.

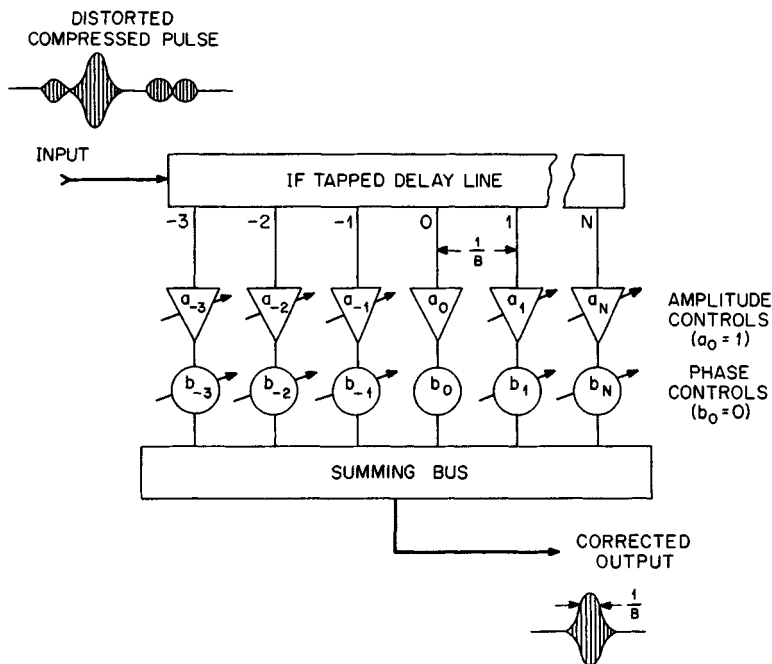


FIG. 10.21 Transversal filter.

that an amplitude ripple results in time sidelobes around the compressed pulse. Pair 8 of Table 10.7 shows that a phase ripple also results in time sidelobes around the compressed pulse. Figure 10.20 shows the amplitude and phase tolerances versus sidelobe level. To obtain time sidelobes of 40 dB below the compressed pulse, the amplitude and phase tolerances are 2 percent and  $1.15^\circ$ , respectively.

**Equalization.** The transversal filter<sup>51,52</sup> is widely used in the equalization of cumulative amplitude and phase distortion. One version of the transversal filter is shown in Fig. 10.21. It consists of a wideband, dispersion-free IF tapped delay line connected through each of its taps to a summing bus by amplitude and phase controls. The zeroth tap couples the distorted compressed pulse, unchanged except for delay, to the bus. The other taps make it possible to "buck out" distortion echoes of arbitrary phase and amplitude over a compensation interval equal to the total line delay. Reducing time sidelobes to an acceptable level is in effect synthesizing an equalizing filter, which makes the spectrum of the output pulse approach the ideal one described above. Because the transversal filter provides the means for reducing time sidelobes, it eliminates the need for a separate weighting filter since frequency weighting (see pairs 3 and 4 of Table 10.7) can be incorporated in the filter.

## REFERENCES

1. Delay Devices for Pulse Compression Radar, *IEE (London) Conf. Publ.* 20, February 1966.
2. Murakami, T.: Optimum Waveform Study for Coherent Pulse Doppler, *RCA Final Rept.*, prepared for Office of Naval Research, Contract Nonr 4649(00)(x), Feb. 28, 1965. AD641391.
3. Morgan, D. P.: Surface Acoustic Wave Devices and Applications, *Ultrasonics*, vol. 11, pp. 121-131, 1973.
4. Eber, L. O., and H. H. Soule, Jr.: Digital Generation of Wideband LFM Waveforms, *IEEE Int. Radar Conf. Rec.*, pp. 170-175, 1975.
5. Hartt, J. K., and L. F. Sheats: Application of Pipeline FFT Technology in Radar Signal and Data Processing, *EASCON Rec.*, pp. 216-221, 1971; reprinted in David K. Barton, *Radars*, vol. 3, Books on Demand UMI, Ann Arbor, Michigan, 1975.
6. Caputi, W. J., Jr.: Stretch: A Time-Transformation Technique, *IEEE Trans.*, vol. AES-7, pp. 269-278, March 1971.
7. Gautier, H., and P. Tournois: Signal Processing Using Surface-Acoustic-Wave and Digital Components, *IEE Proc.*, vol. 127, pt. F, pp. 92-93, April 1980.
8. Slobodnik, A. J., Jr.: Surface Acoustic Waves and SAW Materials, *Proc. IEEE*, vol. 64, pp. 581-594, May 1976.
9. Bristol, T. W.: Acoustic Surface-Wave-Device Applications, *Microwave J.*, vol. 17, pp. 25-27, January 1974.
10. Williamson, R. C.: Properties and Applications of Reflective-Array Devices, *Proc. IEEE*, vol. 64, pp. 702-703, May 1976.
11. Judd, G. W.: Technique for Realizing Low Time Sidelobe Levels in Small Compression Ratio Chirp Waveforms, *Proc. IEEE Ultrasonics Symp.*, pp. 478-481, 1973.
12. Coquin, G. A., T. R. Meeker, and A. H. Meitzler: Attenuation of Longitudinal and Flexural Wave Motions in Strips, *IEEE Trans.*, vol. SU-12, pp. 65-70, June 1965.
13. May, J. E., Jr.: Ultrasonic Traveling-Wave Devices for Communications, *IEEE Spectrum*, vol. 2, pp. 73-85, October 1965.
14. Eveleth, J. H.: A Survey of Ultrasonic Delay Lines Operating Below 100 Mc/s, *Proc. IEEE*, vol. 53, pp. 1406-1428, October 1965.
15. Improved Delay Line Technique Study, *RADC Tech. Rept. RADC-TR-65-45*, May 1965. ASTIA AD617693.
16. Coquin, G. A., and R. Tsu: Theory and Performance of Perpendicular Diffraction Delay Lines, *Proc. IEEE*, vol. 53, pp. 581-591, June 1965.
17. Rodrigue, G. P.: Microwave Solid-State Delay Line, *Proc. IEEE*, vol. 53, pp. 1428-1437, October 1965.
18. O'Meara, T. R.: The Synthesis of "Band-Pass," All-Pass, Time Delay Networks with Graphical Approximation Techniques, *Hughes Aircraft Co. Res. Rept.* 114, June 1959.
19. Peebles, P. Z., Jr.: Design of a 100:1 Linear Delay Pulse Compression Filter and System, master thesis, Drexel Institute of Technology, Philadelphia, December 1962.
20. Hewett, H. S.: Highly Accurate Compression Filter Design Technique, *Stanford University, Electron. Lab. Tech. Rept.* 1965-3, November 1967. See also H. S. Hewett: A Computer Designed, 720 to 1 Microwave Compression Filter, *IEEE Trans.*, vol. MTT-15, pp. 687-694, December 1967.
21. Barker, R. H.: Group Synchronization of Binary Digital Systems, in Jackson, W. (ed.): "Communication Theory," Academic Press, New York, 1953, pp. 273-287.
22. Turyn, R., and J. Stover: On Binary Sequences, *Proc. Am. Math. Soc.*, vol. 12, pp. 394-399, June 1961.

23. Luenburger, D. G.: On Barker Codes of Even Length, *Proc. IEEE*, vol. 51, pp. 230–231, January 1963.
24. Turyn, R.: On Barker Codes of Even Length, *Proc. IEEE* (correspondence), vol. 51, p. 1256, September 1963.
25. Lindner, J.: Binary Sequences Up to Length 40 with Best Possible Autocorrelation Function, *Electron. Lett.*, vol. 11, p. 507, October 1975.
26. Peterson, W. W., and E. J. Weldon, Jr.: "Error Correcting Codes," app. C, M.I.T. Press, Cambridge, Mass., 1972.
27. Golomb, S. W.: "Shift Register Sequences," Holden-Day, Oakland, Calif., 1967, chap. 3.
28. Golay, M. J. E.: Complementary series, *IRE Trans.*, vol. IT-7, pp. 82–87, April 1961.
29. Golay, M. J. E.: Note on complementary series, *Proc. IRE*, vol. 50, p. 84, January 1962.
30. Hollis, E. E.: Another type of complementary series, *IEEE Trans.*, vol. AES-11, pp. 916–920, September 1975.
31. Golomb, S. W., and R. A. Scholtz: Generalized Barker Sequences, *IEEE Trans.*, vol. IT-11, pp. 533–537, October 1965.
32. Somaini, U., and M. H. Ackroyd: Uniform Complex Codes with Low Autocorrelation Sidelobes, *IEEE Trans.*, vol. IT-20, pp. 689–691, September 1974.
33. Frank, R. L.: Polyphase Codes with Good Nonperiodic Correlation Properties, *IEEE Trans.*, vol. IT-9, pp. 43–45, January 1963.
34. Lewis, B. L., and F. F. Kretschmer, Jr.: A New Class of Polyphase Pulse Compression Codes and Techniques, *IEEE Trans.*, vol. AES-17, pp. 364–372, May 1981. (See correction, *IEEE Trans.*, vol. AES-17, p. 726, May 1981.)
35. Rihaczek, A. W.: "Principles of High-Resolution Radar," McGraw-Hill Book Company, New York, 1969, chap. 8.
36. Wheeler, H. A.: The Interpretation of Amplitude and Phase Distortion in Terms of Paired Echoes, *Proc. IRE*, vol. 27, pp. 359–385, June 1939.
37. MacColl, L. A.: unpublished manuscript referred to by H. A. Wheeler (see Ref. 36, p. 359, footnote 1).
38. Burrow, C. R.: Discussion on Paired Echo Distortion Analysis, *Proc. IRE*, vol. 27, p. 384, June 1939.
39. Klauder, J. R., A. C. Price, S. Darlington, and W. J. Albersheim: The Theory and Design of Chirp Radars, *Bell Syst. Tech. J.*, vol. 39, pp. 745–808, July 1960.
40. Blackman, R. B., and J. W. Tukey: "The Measurement of Power Spectra," Dover Publications, New York, 1958.
41. Temes, C. L.: Sidelobe Suppression in a Range Channel Pulse-Compression Radar, *IRE Trans.*, vol. MIL-6, pp. 162–169, April 1962.
42. Cook, C. E., and M. Bernfield: "Radar Signals: An Introduction to Theory and Application," Academic Press, New York, 1967.
43. Taylor, T. T.: Design of Line-Source Antennas for Narrow Beamwidth and Low Sidelobes, *IRE Trans.*, vol. AP-3, pp. 16–28, January 1955.
44. Dolph, C. L.: A Current Distribution for Broadside Arrays Which Optimizes the Relationship between Beam Width and Sidelobe Level, *Proc. IRE*, vol. 34, pp. 335–348, June 1946.
45. Ramsay, J. F.: Fourier Transforms in Aerial Theory, *Marconi Rev.*, vol. 9, October–December 1946.
46. Cummings, R. D., M. Perry, and D. H. Preist: Calculated Spectra of Distorted Gaussian Pulses, *Microwave J.*, pp. 70–75, April 1965.
47. Mason, S. J., and H. J. Zimmerman: "Electronic Circuits, Signals and Systems," John Wiley & Sons, New York, 1960, p. 237.

48. Spellmire, R. J.: Tables of Taylor Aperture Distributions, *Hughes Aircraft Co., Syst. Dev. Lab. Tech. Mem.* 581, October 1958.
49. Nash, R. T.: Stepped Amplitude Distributions, *IEEE Trans.*, vol. AP-12, pp. 515-516, July 1964.
50. DiFranco, J. V., and W. L. Rubin: Signal Processing Distortion in Radar Systems, *IRE Trans.*, vol. MIL-6, pp. 219-225, April 1962.
51. Kallmann, H. E.: Transversal Filters, *Proc. IRE*, vol. 28, pp. 302-310, July 1940.
52. Pratt, W. R.: Transversal Equalizers for Suppressing Distortion Echoes in Radar Systems, *Proc. Symp. Pulse Compression Techniques*, pp. 119-128, Rome Air Dev. Center, RADC-TDR-62-580, April 1963.